CALIBRATION OF NaI *IN SITU* GAMMA SPECTROSCOPY SYSTEMS

FERNALD ENVIRONMENTAL MANAGEMENT PROJECT
FERNALD, OHIO

OCTOBER 2000

U.S. DEPARTMENT OF ENERGY
FERNALD AREA OFFICE

20310-RP-0006
REVISION A
DRAFT

000001

TABLE OF CONTENTS

LIST OF APPENDICES

LIST OF TABLES

000003

LIST OF ACRONYMS AND ABBREVIATIONS

FEMP	Fernald Environmental Management Project
HPGe	high-purity germanium (detector)
kev	kiloelectrovolts
NaI	sodium iodide
NIST	National Institute of Standards and Technology
pCi/g	picoCuries per gram
ROI	region of interest
RSS	Radiation Scanning System
RTIMP	Real Time Instrumentation Measurement Program
RTRAK	Radiation Tracking System
WAC	waste acceptance criteria

1.0 INTRODUCTION

1

2

3 This report presents an improved method for calibrating the Sodium Iodide (NaI) detectors in the mobile

4 *in situ* gamma spectroscopy systems used for scanning soils for radionuclides at the Fernald

5 Environmental Management Project (FEMP). The improved method is faster, safer, and better at

6 quantifying soil concentrations of radionuclides than the method that has been in use.

7

8 The method that has been used at the FEMP for calibrating NaI detectors relies on field calibration of the

9 detectors using contaminated soil identified at a number of FEMP site locations. Results obtained using

10 HPGe detectors at those locations are used as the calibration standard. The method needs to be replaced

11. for several reasons. As site remediation proceeds, the identified areas are lost, preventing their use in any

12 future calibration efforts. In addition, the contamination at such locations is generally spatially

13 heterogeneous, affecting the quality of the calibrations. Further, correlation between the presence of the

14 different contaminants at these locations has technically complicated the calibration process. By using

15 sealed sources with known characteristics and carrying out calibrations under controlled conditions, all of

16 these problems have been eliminated.

17

18 Two separate methods for calibrating NaI detectors have been evaluated and are discussed in this report.

19 One method involves direct calibration using a calibration pad. The second method involves a point

20 source calibration similar to that used for HPGe detectors at the FEMP. An evaluation of the results

21 provided by the two methods indicates that calibration using the pad provides similar, but superior,

22 results.

23

24 The regions of interest (ROIs) used when analyzing NaI spectral data were re-evaluated during the

25 development of the two calibration methods. The subject is discussed in Section 2.

26

27 The use of a calibration pad is discussed in Section 3, and calibration results are presented for four

28 systems: the Radiation Scanning System 1 (RSS1), RSS2, the Radiation Tracking System (RTRAK), and

29 the Gator. Except for the RSS2, all of these systems had been previously calibrated using the field

30 method.

31

32 An evaluation of the calibration results obtained using the calibration pad and those obtained using the

33 point source calibration is presented in Section 4.

34

1   Recommendations are presented in Section 5. In particular, it is recommended that future calibrations of

2   the NaI detectors be performed using the calibration pad and that a procedure be established for the

3   calibrations. Conclusions are provided in Section 6.

4

5   Considerable supporting material is included in the appendices. The theoretical background for the

6   design and use of the calibration pad is provided, as is the theoretical background for point source

7   calibrations. Detailed descriptions of the sources used in the calibration pad are provided.

2.0 REGIONS OF INTEREST

ROIs are used when analyzing the NaI spectral data. ROIs consist of a range of channels (gamma energies) that are normally set to encompass as much as the peak from the isotope of concern as possible. However, the effect of interfering isotopes must also be considered when the ROIs are established.

As part of this calibration effort, the ROIs were re-evaluated to determine if any adjustments should be made. The uranium ROIs were subsequently adjusted slightly to help eliminate interference from thorium before the calibrations were performed. During the calibration process, a further evaluation determined that widening the radium ROI would not greatly affect the interference but would improve efficiency. The original and the new ROIs, expressed in terms of channel numbers, are included in Table 2-1. The NaI spectrum uses 512 channels numbered from zero to 511, which represent an energy range from zero to approximately 3000 kiloelectrovolts (kev).

Previous field data were reanalyzed using the different calibrations to evaluate the effectiveness of the new ROIs. The results are discussed in Section 4 of this report. A simple evaluation was performed in which the net count rate of each isotope of concern was plotted against the high purity germanium (HPGe) activity for every location. This was done for both the new and the original ROIs. Since each isotope interfered with the other isotopes, coefficients produced from a simple linear regression were meaningless. However, the R^2 value, demonstrating the goodness of the fit, was useful since the better the fit (R^2 closer to one), the less dependent the net count rate was on other isotopes.

The regression was performed for each isotope for the data plotted in Section 4. The values of these data are shown in Appendix E. Data existed only for the RSS1, the RTRAK, and the Gator. Only uranium and radium isotopes were evaluated since those were the only ROIs that were modified. Table 2-2 shows the R^2 values.

It can be seen that in nearly every case, the new ROIs produced responses that were more closely related to the isotopes being measured and therefore reduced the effects of interference.

TABLE 2-1
REGIONS OF INTEREST FOR NaI DETECTORS

	Uranium			Radium			Thorium		
	Isotope	Bkg low	Bkg high	Isotope	Bkg low	Bkg high	Isotope	Bkg low	Bkg high
Original	161-180	142-147	181-186	290-316	284-289	317-322	411-483	405-410	484-489
New	161-178	155-160	179-184	282-350	276-281	351-356	411-483	405-410	484-489

TABLE 2-2
R^2 VALUES FOR REGIONS OF INTEREST

	Original Uranium	New Uranium	Original Radium	New Radium
RSS1	0.7074	0.9828	0.9922	0.9746
RTRAK	0.5434	0.8664	0.7427	0.9805
Gator	0.383	0.9887	0.9128	0.9841

1   **3.0 CALIBRATION OF NaI DETECTORS USING A CALIBRATION PAD**

2

3   3.1 <u>DESCRIPTION OF METHOD</u>

4   A detailed description of this method is included in Attachment A. This section summarizes the

5   calibration process and results.

6

7   The calibration was conducted by producing a calibration pad of known concentration and in the same

8   geometry in which the field measurements were taken. The detector's response to this known

9   concentration was then used to determine the calibration factors. Since NaI detectors are calibrated for an

10   infinitely large homogeneous source, FEMP personnel simulated a large homogeneous source by

11   manufacturing a smaller pad and distributing discrete sources in a specific pattern. With known sources

12   in a known pattern, it was possible to determine an effective concentration as if the pad had been

13   infinitely large. The details of this process are provided in Appendix B.

14

15   NaI calibration consisted of efficiency determination and the interference coefficients. The interference

16   coefficients were necessary because most of the isotopes of interest produced gammas of various

17   energies, which in turn produced a detector response in areas of the spectrum that were in or near other

18   ROIs. To account for this, sources of the same isotopes of interest were counted, and the net count rate of

19   each isotope was calculated as normal. A ratio of these count rates was then used as a correction factor,

20   which was positive or negative, to remove the effect of the interfering isotope.

21

22   The efficiency determination is the ratio of the detector response to the known concentration of a

23   particular isotope. The concentration could be reported confidence that no interference exists from other

24   isotopes since known sources were used.

25

26   3.2 <u>CALIBRATION SOURCES</u>

27   In order to determine the efficiency and the interference coefficients, sources containing the isotopes of

28   concern were required. The sources utilized for this evolution were uranium-238, radium-226, and

29   thorium-232. The sources were manufactured at the FEMP because of the difficulty in obtaining National

30   Institute of Standards and Technology (NIST)-traceable standards of these isotopes in equilibrium with

31   their progeny and because of the amount of source material required. Even with a reduced pad size, the

32   required amount of source material was greater then 60 pounds. A detailed discussion of the

33   manufacturing and assay of these sources is included in Appendix C, including an assessment of the

1 effective concentration of the pad based on the source activity. The source placement pattern is described

2 in Appendix B.

3

4 Each source consisted of source material loaded into a plastic tube 6 inches long and 1.25 inches in

5 diameter. These sources were then placed in additional plastic tubes inserted into the calibration pad. In

6 this manner, the sources of one isotope could be easily removed and replaced with the sources of another

7 isotope. The source pattern consisted of 45 sources of each isotope distributed in a 360-degree circular

8 pattern. When the outer tubes were inserted into the pad, the soil that was removed was placed into

9 additional tubes similar to the source tubes. This soil was used fill the holes during background counts.

10

11 Table 3-1 lists each isotope, the average concentration within each type of source tube, and the effective

12 concentration when all 45 sources were inserted into the pad.

13

14 3.3 RESULTS

15 3.3.1 Efficiency

16 Once the effective concentrations of the individual isotopes were determined, the sources were counted

17 with the NaI detector. Each detector was centered over the pattern and a spectrum was acquired for

18 5 minutes. The isotope sources were then exchanged and the process repeated until a spectrum had been

19 collected of each isotope and a background reading. Since the concentrations of other isotopes in the

20 sources were small if not zero, no interference correction was necessary. The net count rate was divided

21 by the effective pad concentration to determine the efficiency as a ratio of net counts per second to

22 picoCuries per gram (pCi/g). This will be useful when future field counts are obtained since the

23 interference-corrected net count rate of each isotope can simply be divided by the appropriate efficiency

24 in order to obtain the concentration in pCi/g. The efficiency for each detector calibrated is included in

25 Table 3-2 along with the one standard deviation counting error.

26

27 3.3.2 Interference Coefficients

28 Most of the isotopes of concern emit multiple gamma of different energies. Because of this, some gamma

29 rays emitted by one isotope appeared in another isotope's ROI. Thirteen interference coefficients were

30 used to correct for these interfering gammas. Once the count rate from one isotope was determined, it

31 was multiplied by the appropriate interference coefficient to determine its interference on another

32 isotope's ROI. The equations used to determine the interference-corrected net count rates are shown

33 below.

1    $U_{(corr)} = F1 * U_{(raw)} + F2 * Ra_{(raw)} + F3 * Th_{(raw)}$
2    $Ra_{(corr)} = F4 * U_{(raw)} + F5 * Ra_{(raw)} + F6 * Th_{(raw)}$
3    $Th_{(corr)} = F7 * U_{(raw)} + F8 * Ra_{(raw)} + F9 * Th_{(raw)}$
4    $K_{(corr)} = F10 * K_{(raw)} + F11 * U_{(raw)} + F12 * Ra_{(raw)} + F13 * Th_{(raw)}$

5   Equation 3-1

6

7   The "corr" subscript indicates the interference-corrected net count rate and the "raw" subscript indicates

8   the raw net count rate.

9

10   Since an isotope cannot "interfere" with itself, some of these interference coefficients were expected to

11   equal one. However, the net count rates to which the coefficients were applied were also subjected to

12   interference; therefore, a set of equations were solved simultaneously to get the appropriate coefficients.

13   As a result, the values of F1, F5, and F9 above are not exactly equal to one. Potassium-40, on the other

14   hand, emits only one gamma energy and thus does not interfere with the other isotopes. Therefore, it is

15   not necessary to include potassium-40 in the set of simultaneous equations and the subsequent value of

16   F10 is equal to one. The solutions of these equations and the interference coefficients are included in

17   Appendix A.

18

19   The calculated values of these 13 interference coefficients for each instrument are shown in Table 3-3.

20   The table includes the one sigma counting error. As already noted, F1, F5, and F9 were nearly, but not

21   exactly, equal to one. The other values in the table indicate the amount of interference caused on one

22   isotope by other. For example, in the case of the RSS uranium equation, F2 indicates that in order to

23   correct the uranium net counts for interference, approximately 16.5 percent of the raw radium-226 net

24   counts were added to the uranium net counts. F3 indicates that approximately 0.6 percent of the raw

25   thorium-232 net counts were subtracted from the uranium net counts. The decision to add or subtract

26   depended on the major interfering energies from some isotopes: some appeared in background regions,

27   while others appeared in the actual ROI. The background region was used to determine the background

28   in that area of the spectrum. When this is elevated by interference, the background subtraction is

29   overestimated and the net counts are artificially low.

30

31   The major factors that affected these coefficients were detector resolution, detector efficiency response,

32   and the construction of the detector and its housing. Since these coefficients were ratios of different

33   ROIs, they were affected by anything that would normally affect different energy gamma rays, as well as

34   anything that would affect the detectors' responses to those gamma rays. For example, if detectors A

35   and B had the same efficiency for the high energies but different efficiencies for the lower energies, the

36   coefficients would have been different. Similarly, the detector resolution was a measure of the width of

1   the gamma ray peak. With different resolutions between detectors, a different fraction of a peak would

2   have been included in a particular ROI and thus change the coefficients. Any shielding between the

3   source and the detector also affected different energy gamma rays differently. Since each detector had its

4   own housing, it was possible for each to exhibit very different shielding characteristics and thus produce

5   different coefficients, even a differently signed coefficient.

6

7   3.3.3 <u>Potassium-40</u>

8   Potassium-40 is a naturally occurring isotope found in most soil. It has no regulatory purpose at the

9   FEMP, but is a dependable isotope that can be used as an indicator of the detector performance. Because

10   of this, calibration coefficients were derived for potassium-40 but without the rigor that was used in

11   determining coefficients for the other isotopes. Since potassium-40, uranium-238, radium-226 and

12   thorium-232 all affect the potassium-40 ROI, it was necessary to develop coefficients for each.

13

14   The natural potassium-40 in the calibration pad was used as the source to determine calibration efficiency.

15   This value was assayed using an HPGe detector set at the same height as the NaI detector. The remaining

16   interference coefficients for potassium-40 were determined in the same manner as the other isotopes.

17

18   3.3.4 <u>Calibration Factors</u>

19   Each spectrum was analyzed by determining the raw net count rate from each isotope, applying the

20   interference correction using the values in Table 3-3, and then dividing this corrected count rate by the

21   efficiency. In the future, this process could be simplified somewhat for field use by simply dividing the

22   interference coefficients by the efficiency. This provides coefficients for multiplying the raw net count

23   rates by in order to obtain the final results directly. The coefficients resulting from this process, along

24   with the one sigma counting error, are listed in Table 3-4.

25

26   These factors were then used just as the values of F1 through F13 were used in Equation 3-1 except that

27   the results are in pCi/g instead of corrected net counts per second. Section 4 of this report describes the

28   efforts performed to verify this calibration.

TABLE 3-1
DIRECT CALIBRATION SOURCE DATA

Isotope	Source material concentration (pCi/g)	Effective pad concentration (pCi/g)
U-238	1.56E5 ± 4.04E3	326.5 ± 8.43
Ra-226	11209 ± 280	20.37 ± 0.51
Th-232	5295 ± 194	9.045 ± 0.331

TABLE 3-2
EFFICIENCIES DETERMINED BY DIRECT CALIBRATION

Isotope	Energy (kev)	RSS1	RSS2	RTRAK	Gator
U-238	1001	0.261±.004	0.221±.004	0.190±.004	0.109±.004
Ra-226	1765	7.672±.117	9.291±.111	8.077±.108	6.863±.109
Th-232	2614	13.199±.137	13.253±.144	12.019±.137	11.184±.135
K-40	1460	5.184±.082	4.893±.084	4.499±.082	3.668±.087

TABLE 3-3
DIRECT CALIBRATION INTERFERENCE COEFFICIENTS

	RSS	RSS2	RTRAK	Gator
F1	0.982±.002	1.018±.004	1.007±.003	1.005±.003
F2	0.165±.010	-0.073±.008	-0.033±.009	-0.019±.010
F3	-0.006±.013	-0.454±.014	-0.425±.014	-0.130±.014
F4	-0.111±.012	-0.130±.015	-0.088±.016	-0.154±.030
F5	1.001±.004	1.000±.003	1.001±.003	1.028±.004
F6	0.525±.018	0.493±.019	0.483±.020	0.451±.021
F7	-0.009±.006	-0.017±.007	-0.009±.008	-0.028±.015
F8	0.036±.006	-0.020±.004	-0.003±.005	0.059±.007
F9	1.019±.003	0.998±.004	1.002±.004	1.028±.004
F10	1.000	1.000	1.000	1.000
F11	0.003±.017	-0.047±.017	-0.041±.024	-0.092±.045
F12	-0.303±.017	-0.132±.014	-0.118±.016	-0.072±.020
F13	-0.027±.015	0.111±.013	0.109±.016	0.018±.017

TABLE 3-4
CALIBRATION FACTORS DETERMINED BY DIRECT CALIBRATION

		RSS	RSS 2	RTRAK	Gator
U equation	U coefficient	3.767±.054	4.602±.082	5.311±.102	9.185±.296
	Ra coefficient	0.633±.039	-0.331±.037	-0.175±.047	-0.172±.093
	Th coefficient	-0.021±.050	-2.054±.071	-2.243±.086	-1.184±.135
Ra equation	U coefficient	-0.014±.002	-0.014±.002	-0.011±.002	-0.022±.004
	Ra coefficient	0.130±.002	0.108±.001	0.124±.002	0.150±.002
	Th coefficient	0.068±.003	0.053±.002	0.060±.003	0.066±.003
Th equation	U coefficient	-0.001±.000	-0.001±.001	-0.001±.001	-0.003±.001
	Ra coefficient	0.003±.000	-0.001±.000	0.000±.000	0.005±.001
	Th coefficient	0.077±.001	0.075±.001	0.083±.001	0.092±.001
K equation	K coefficient	0.193±.003	0.204±.004	0.222±.004	0.273±.006
	U coefficient	0.001±.003	-0.010±.004	-0.009±.005	-0.025±.012
	Ra coefficient	-0.058±.003	-0.027±.003	-0.026±.004	-0.020±.005
	Th coefficient	-0.005±.003	0.023±.003	0.024±.004	0.005±.005

4.0 VERIFICATION AND EVALUATION OF CALIBRATION RESULTS

This report discusses two different methods for the direct calibration of *in situ* NaI detectors, pad calibration and point calibration. These two methods use:

- Different theories and sources for efficiency determinations.
- The same sources for determining interference coefficients.

Interference determinations were determined using the same sources as a matter of expediency because the point source calibration only requires a strong source of each isotope of interest without regard to its strength. The pad calibration sources met this requirement. This requirement also implies that the sources are free of significant impurity isotopes. The gamma spectroscopy analysis performed as part of the source assay, see Appendix C, shows that no significant impurities exist in these sources.

During this calibration effort, it has been assumed that if two completely independent methods provide comparable results, then the methods essentially validate each other. The pad and point calibration methods are not completely independent of each other because the pad calibration sources are used to determine interference coefficients for both methods. However, it must be kept in mind that the only requirement for interference correction for the point source method is a strong source of each nuclide of interest.

The final product of ether calibration is a set of coefficients. These coefficients are multiplied by the raw net count rate of each isotope to eliminate any interference from other isotopes and to convert the net count rate into pCi/g. Mathematically this looks like the following.

$$U(pCi/g) = F1*U(cps) + F2*Ra(cps) + F3*Th(cps)$$
$$Ra(pCi/g) = F4*U(cps) + F5*Ra(cps) + F6*Th(cps)$$
$$Th(pCi/g) = F7*U(cps) + F8*Ra(cps) + F9*Th(cps)$$
$$K(pCi/g) = F10*K(cps) + F11*U(cps) + F12*Ra(cps) + F13*Th(cps)$$

Equation 4-1

Where:
X(pCi/g) = Soil activity of isotope "X" in pCi/g
X(cps) = Raw net count rate for isotope "X" in counts per second
Fx   = The calibration coefficient (13 in all)

1   4.1 METHODS USED TO EVALUATE CALIBRATION

2   These two calibration methods were compared using the following methods. The comparison is

3   presented in separate subsections for each NaI instrument.

4

5   4.1.1 Coefficient Comparison

6   The calibration results were determined by subtracting one coefficient from the other; the degree of

7   agreement can be judged by how close this difference is to zero. The standard deviation of the difference

8   was determined from counting error of each coefficient. Any difference that fell within two standard

9   deviations of zero could be said to be similar at the 95 percent confidence level. It should be noted at this

10 point that these counting errors represent only an approximation. They were propagated with the

11 assumption that no correlation exists between the uncertainty of the various terms. If a correlation did

12 exist, covariance terms would have to be included and could cause the calculated uncertainty to increase

13 or decrease.

14

15 4.1.2 Evaluation of Point Source Calibration Using the Calibration Pad

16 When the statistical comparison was performed, many of the factors agreed but some fell outside this

17 band, requiring further evaluation. This was done by utilizing the pad calibration spectra. Since the point

18 source calibration was independent of these spectra, a detailed analysis was conducted to compare the

19 values produced by the point source calibration to the theoretical values of the calibration pad. This

20 process indicated that whenever the coefficients did not match, it was because the point source calibration

21 was inaccurate.

22

23 4.1.3 Check of Previous Field Data Using the New Calibrations

24 Finally, as a field check of the calibration, some field data were analyzed and compared to HPGe values

25 obtained in the same location. Plots of this comparison are included in this section and the data are listed

26 in Appendix E. Appendix E also includes a discussion of four data points that were excluded from the

27 data set. In order to perform a good field check of this calibration, it would be highly desirable to find

28 some field locations that are relatively homogeneous, without any large sources of shine radiation and

29 with various degrees of contamination. The lack of locations meeting these criteria was one of the

30 primary reasons for developing the pad calibration technique. While some locations may not be adequate

31 for instrument calibration, they may be sufficient for determining calibration adequacy. The original

32 calibration data were subsequently used, as well as a number of points that were removed from that

33 calibration as outliers plus a few additional points obtained since then. These spectra were analyzed using

34 the point source calibration, the pad calibration, and the original calibration coefficients. The values

1   obtained from these spectra were then plotted against an HPGe measurement taken in the same location

2   on the same day. While a moisture correction would normally be applied to the data, it was not done for

3   this comparison in order to remove any potential variability in moisture indications. In addition, for all

4   primary isotopes of concern, the HPGe uses an average of several different gamma energies coming from

5   the isotope of interest while the NaI instruments use only one. In an attempt to reduce inconsistencies that

6   could be caused by heterogeneous contamination, the HPGe values recorded here were only from the one

7   gamma energy that the NaI instruments used.

8

9   4.2 RSS1

10 Table 4-1 shows the individual factors derived from both the point source calibration and the pad

11 calibration including their two sigma counting error. Table 4-1 includes the difference between the two,

12 along with the two sigma counting error associated with that difference.

13

14 It can be seen from the last column that several of the factors agreed. The ones that did not agree with a

15 95 percent confidence are F1, F3, F8, F9, and F13. These five coefficients will require further evaluation,

16 possibly by applying these factors to actual spectra. The best-characterized spectra were the four spectra

17 collected for the pad calibration. Table 4-2 shows the theoretical value for each isotope for each spectrum

18 as well as the measured HPGe value and the calculated NaI value using the point calibration coefficients

19 and the pad calibration coefficients. All the values in the table are in pCi/g.

20
21 In evaluating the performance of the individual calibrations, it must be noted that these spectra were the

22 actual spectra from which the pad calibration was derived. For this reason, it was inappropriate to

23 evaluate the pad calibration factors using these spectra; however, they were appropriate for evaluating the

24 point calibration coefficients. In fact, evaluating these values against the theoretical values for the

25 calibration pad was a completely independent verification of these values.

26

27 The first factor to be evaluated, F1, was the uranium coefficient in the uranium equation. This was

28 evaluated by comparing the theoretical uranium value when the uranium sources are used with the

29 calculated uranium value from the same spectrum. The calculated value of uranium was very close to the

30 theoretical value (348.4 pCi/g and 326.5pCi/g) and indeed appeared to produce adequate results.

31 However, the values of F1 from the two calibrations were also relatively close, but not statistically the

32 same. The calculated uranium value was approximately 6.7 percent higher than the theoretical value. If

33 the value of F1 obtained from the point source calibration were reduced by 6.7 percent, the new value

1 would become 3.814. When compared to the pad source calibration value of F1 (3.767), the F1 value

2 obtained from the pad calibration provided a better calibration factor.

3

4 The F3 value was the thorium coefficient for the uranium equation. This value was multiplied by the

5 thorium net count rate to correct the uranium net count rate for interference caused by thorium. This

6 factor was evaluated using the uranium values calculated from the point source calibration for the

7 background spectrum and the spectrum from the thorium sources. The only difference between these

8 spectra was caused by thorium. The uranium concentration was 39.24 pCi/g lower when the thorium was

9 increased by 9.045 pCi/g. This indicates that the F3 coefficient was lowering the uranium concentration

10 more than it should or, in other words, the coefficient was too negative. This analysis was somewhat

11 complicated by the fact that the value for F1 should have been obtained from the pad calibration. When

12 only this value was changed, the uranium concentration was approximately 43 pCi/g lower (instead of

13 39 pCi/g) when the thorium was elevated. A detailed analysis of the net count rates obtained from the

14 spectra indicates that the point source value for F3 should have been less negative by approximately

15 0.3585. Thus the new value for F3 was equal to -0.0725, which was statistically the same as the F3 value

16 obtained from the pad calibration.

17

18 The value of F9 was the thorium coefficient for the thorium equation. The primary coefficient was

19 determined to be correct before evaluating any secondary coefficients. F9 was evaluated using the

20 theoretical thorium value when the thorium sources were used with the calculated thorium value from the

21 same spectrum. While the theoretical value of thorium is 9.045 pCi/g, the calculated value increases only

22 8.42 pCi/g above background. This indicates that the value of F9 for the point source calibration was

23 larger by 6.96 percent. This increase made the F9 value for the point calibration 0.076, which was within

24 statistical uncertainty of the F9 value from the pad calibration.

25

26 The factor F8 was the radium coefficient for the thorium equation. The coefficient attempted to remove

27 the radium interference from the net thorium count rate and thus could be evaluated using the background

28 spectrum and the radium source spectrum. These spectra indicated that when the radium value was

29 increased, the calculated thorium value decreased even though the theoretical value of thorium was

30 constant. This indicates that the point source calibration value for F8 should be higher. A detailed

31 evaluation using the pad calibration value for F9 indicated that the accurate value of F8 should have been

32 0.00277. While the table showed only a rounded off value for F8, the true value for the pad calibration

33 was 0.00272. This was a difference of 0.00005 ± 0.00057, indicating that the values were statistically the

34 same.

1   F13 was the thorium coefficient for the potassium equation. This was established using the background

2   spectrum and the thorium source spectrum. It was obvious by looking at the calculated potassium values

3   that too much was added to the potassium calculation when thorium was present. This indicated that the

4   value for F13 in the point source calibration was too high. An analysis of the net count rates indicated

5   that the value should have been lowered by 0.040, making the new value -0.004. The new value was well

6   within the statistical variation of the pad calibration value for F13, which was -0.005.

7

8   The overall result of this comparison indicates that the values for eight of the 13 coefficients are

9   statistically similar. A more in-depth analysis indicated that in every case, the remaining five coefficients

10 are inaccurate for the point calibration and that the degree and direction required to correct them brings

11 them in line with the pad calibration. Since it would be unlikely for two different theories to produce the

12 same coefficients by chance, the values of the eight coefficients that agree must be believed to be

13 accurate. The detailed analysis indicates that the point source calibration is likely inaccurate for the

14 remaining five.

15

16 The following graphs show uranium, radium, and thorium values calculated and plotted against the HPGe

17 value for each location. The HPGe values were also plotted against themselves, giving a clear straight

18 line indicating the location of a perfect match. The data plotted here are included in Attachment F, which

19 also provides a discussion of four data points eliminated from the set.

RSS1 U-238

000019

RSS1 Ra-226

1
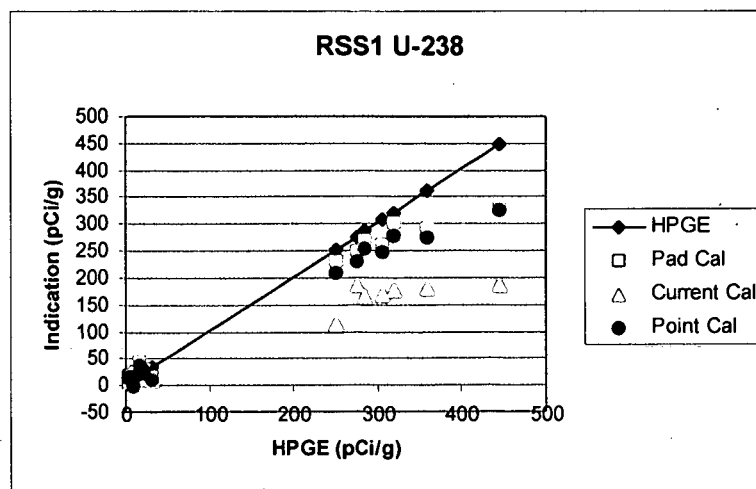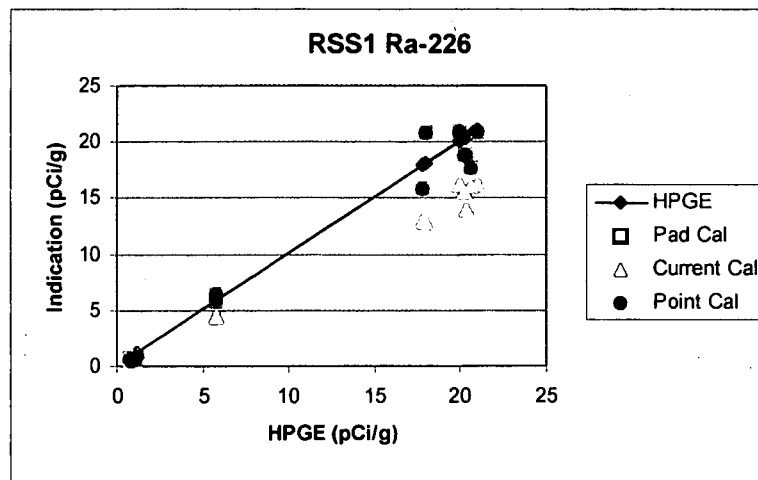
2   The plots indicate that there were a number of outliers for all the calibrations. Both the point calibration

3   and the pad calibration performed better than the original calibration in nearly every case. The degree of

4   agreement between the point source calibration and the pad calibration demonstrates very effectively that

5   that the two different theories produced comparable results. This implies the two theories are capable of

6   validating each other and that both the point source and the pad calibrations are adequate calibration

7   methods for the RSS.

8

9   4.3 RSS2

10   The RSS2 is a new instrument that has never been calibrated. Consequently, there were no field data to

11   use as a basis for comparison. However, the comparison of the two calibration coefficients, as well as a

12   test of the point source calibration on the pad spectra, can be performed.

13

RSS1 Th-232
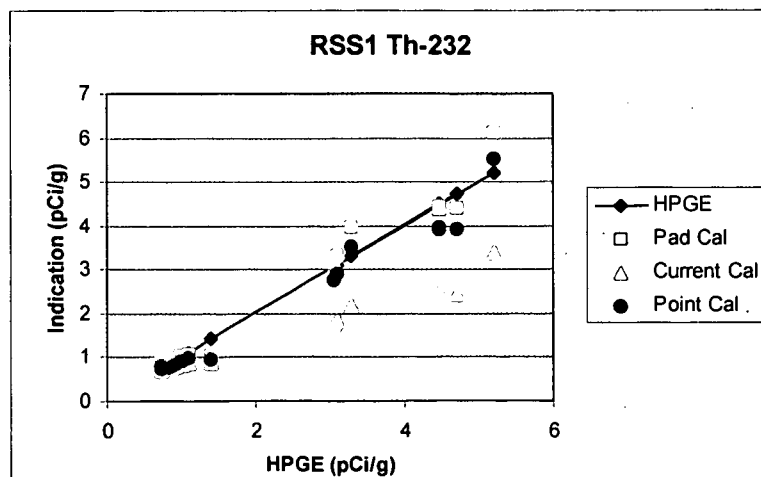
1   Table 4-3 indicates that factors F1, F2, F10, and F12 did not agree at the 95 percent confidence level.

2   That is, the difference between the values obtained with the two calibrations were not within 2 standard

3   deviations of zero. Under the RSS1 section of this report, the factors that did not agree were further

4   evaluated by analyzing the pad calibration spectra using both calibrations. Table 4-4 shows the results of

5   analyzing these spectra.

6

7   At this point, an evaluation of the point source calibration was performed using the above data. This

8   evaluation was limited to the factors that did not match the pad calibration factors, i.e., F1, F2, F10,

9   and F12.

10

11   It can be seen from the above data that while the theoretical value of uranium was 326.5 pCi/g, the point

12   source calibration produced a value of 262.18 pCi/g. This means the point source value for F1 was only

13   80.3 percent of what it should have been. If the value of F1 were adjusted for this, the new value would

14   have been 4.793, which was statistically the same as the pad calibration value of 4.602.

15

16   The value of F2 was evaluated using the background spectrum and the spectrum with radium sources

17   loaded into the pad. The uranium value increased by 18.45 pCi/g when only a radium source was added

18   to the pad. This indicated that the radium coefficient did not subtract enough to account for the radium

19   interference. A detailed analysis of the net count rates, using the F1 coefficient from the pad calibration,

20   indicated the correct value for F2 should have been -0.333, which was very close to the pad calibration

21   value of -0.331.

22

23   F10 was evaluated using the potassium value calculated from the background spectrum. The point source

24   calibration calculated a value of 6.91 pCi/g, while the HPGe indicated a value of 8.28 pCi/g. This

25   indicated that the point source value for F10 is only 83.5 percent of what it should have been. If the value

26   of F10 were adjusted for this, the new value would have been 0.199, which is statistically the same as the

27   pad calibration value of 0.204.

28

29   The last value, F12, was evaluated using the background spectrum and the spectrum with radium source

30   loaded into the pad. This indicated that radium sources caused the calculated potassium value to decrease

31   by 2.98 pCi/g so the point source calibration value of F12 must have been subtracting too much. A

32   detailed analysis of the net count rates using the new value for F10 indicated that the correct value for

33   F12 is –0.032. This value was within the two standard deviation range of the pad calibration value for

34   F12 of –0.027.

1   This analysis indicated that the point source calibration values for the RSS2 match all but four of the pad

2   calibration factors for it. The detailed analysis above indicated that where a mismatch occurred, the point

3   source values were inaccurate. Since the RSS2 is a new instrument, there were no field data to check the

4   pad calibration. However, it is unrealistic to believe these two theories of calibration could produce

5   similarly incorrect answers. That implies nine of the 13 coefficients are accurate, and the remaining four

6   can be proven to be inaccurate for the point source calibration.

7

8   ## 4.4 RTRAK

9   As with the RSS1, the evaluation of the RTRAK calibration will start with a comparison of the calibration

10   factors. Again the difference obtained by subtracting one factor from the other is included.

11

12   It can be seen from the last column of Table 4-5 that factors F1, F4, F6, F11, and F13 did not agree at the

13   95 percent confidence level. That is, the difference between these values obtained with the two

14   calibrations were not within two standard deviations of zero. Under the RSS1 section of this report, the

15   factors that did not agree were further evaluated by analyzing the pad calibration spectra using both

16   calibrations. The RTRAK data were evaluated in the same manner. Table 4-6 shows the results of

17   analyzing these spectra.

18

19   An analysis was conducted by comparing the point source calibration derived values to the theoretical

20   values for the pad spectra is to determine which coefficients were correct.

21

22   The evaluation of F1 involved comparing the theoretical to the calculated uranium value when the

23   uranium source was in the pad. The theoretical value was 326.5 pCi/g while the point source calibration

24   calculated value was 243.84 pCi/g. This means the point source value for F1 was only 74.7 percent of

25   what it should have been. If the value of F1 were adjusted for this, the new value would have been 5.479,

26   which was statistically the same as the pad calibration value of 5.311.

27

28   The F4 value was the uranium coefficient for the radium equation. It was evaluated using the background

29   spectrum and the uranium source spectrum. These spectra indicate that when the uranium sources were

30   added to the pad, the calculated radium value decreased by 3.76 pCi/g. This implies the point source

31   value for F4 was subtracting too much. An analysis of the net count rates indicated that the point source

32   value of F4 should have been less negative by 0.061, making the new value –0.012, which was obviously

33   close to the pad calibration value of –0.011.

34

1 F6 was the thorium coefficient for the radium equation and was evaluated using the background spectrum

2 and the thorium source spectrum. These spectra indicated that when the thorium sources were added to

3 the pad, the calculated radium value increased by 3.81 pCi/g. This implies the point source value for F6

4 was adding too much. An analysis of the net count rates indicated that the point source value of F6

5 should have been lower by 0.017, making the new value 0.091. This value, however, was still not

6 statistically the same as the pad calibration value of 0.060. The problem was determined to be the F4

7 value. Since thorium produced a number of counts in the uranium region, even with a correct value for

8 F6, the radium value could have been miscalculated if the value for F4 was inaccurate. Since the value of

9 F4 was already shown to be inaccurate, this process was repeated but the pad calibration value of F4 was

10 used. With this value replaced, the calculated values for radium were 0.76 pCi/g for the background

11 spectrum and 5.34 pCi/g for the thorium spectrum. The subsequent analysis of the net count rates

12 indicated that the F6 point source value needed to be lowered by 0.042 for a new value of 0.066, which

13 was statistically the same as the pad calibration value of 0.060.

14

15 The remaining values, F11 and F13, were the uranium and thorium coefficients for the potassium

16 equation. Since uranium causes very little interference with the thorium region, the F11 value was

17 evaluated first and then the F13 value was evaluated using the new value for F11. Using the background

18 and uranium source spectra, the uranium was shown to cause the potassium value to increase by

19 2.41 pCi/g. An evaluation of the net count rates indicated that the F11 value for the point source

20 calibration should have been lower by 0.039, making the new value −0.009, an exact match of the pad

21 calibration value. Replacing the F11 value with the new one and re-calculating the spectra yielded

22 calculated potassium values of 7.76 pCi/g for the background spectrum and 5.32 pCi/g for the thorium

23 source spectrum. This indicated that the F13 value was too low. A recalculated value using the net count

24 rates was 0.024, an exact match for the pad calibration factor.

25

26

1   As a final check on this calibration, the original calibration data, as well as a few other measurements,

2   were plotted on the graphs below. As with the RSS1, the HPGe was also plotted as an indication of the

3   expected value. Also like the RSS1 plot, the HPGe indication was the value obtained only from the one

4   gamma peak used by the NaI instruments.

RTRAK U-238

RTRAK Ra-226

RTRAK Th-232
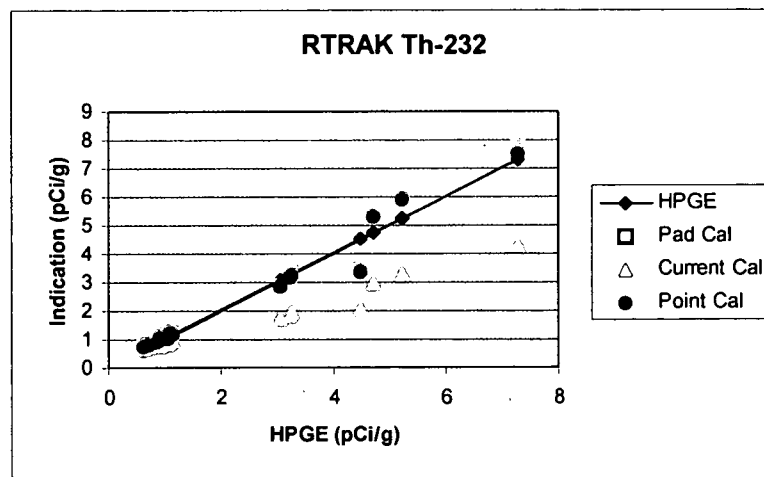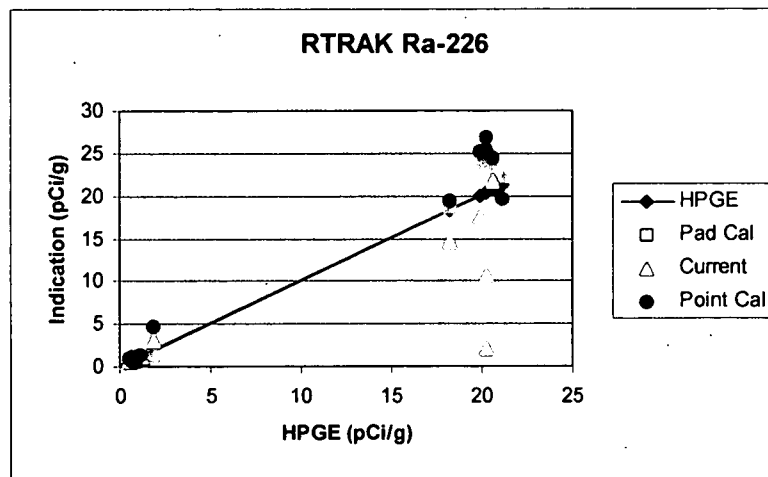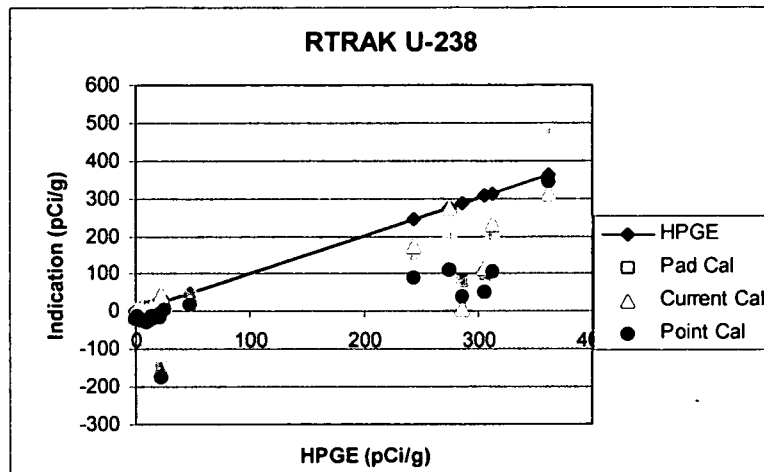
1   As with the RSS1 plots, there were some outliers that were likely caused by the heterogeneous nature of

2   the contamination or by radiation shine from a nearby warehouse. Also like the RSS1, both new

3   calibrations match the HPGe values for thorium and radium closer than the original calibration. This

4   effect is not as clear with the uranium values but what is clear is that every calibration has trouble

5   evaluating some of these spectra. This is evidence that the nature of these locations is very heterogeneous

6   and thus unfriendly to any form of characterization including physical samples. In any case, this analysis

7   shows very well that the pad calibration is an adequate alternative to the current method of calibrating the

8   NaI instruments.

9

10   4.5 <u>GATOR</u>

11   As with the other instruments, an analysis of the Gator calibration began with a list of the calibration

12   coefficients and a determination of whether the difference was within two standard deviations of zero.

13

14   The last column in Table 4-7 indicates that factors F1, F3, F10, and F13 do not agree at the 95 percent

15   confidence level. That is, the difference between these values obtained with the two calibrations were not

16   within 2 standard deviations of zero. As with the other calibrations, the next step was to analyze the pad

17   calibration spectra using both calibrations. The Gator data were evaluated in the same manner, and the

18   results are presented in Table 4-8.

19

20   The most obvious discrepancy was in the point source data, which were clearly lower than the pad

21   calibration data as well as the HPGe results and the theoretical values. This was most noticeable in the

22   primary constituents, i.e., the uranium value with the uranium sources, etc. The uranium values were the

23   largest, followed by the potassium, radium, and then thorium. This also happened to be the order of the

24   gamma ray energies, with uranium being the lowest (1001 kev), followed by potassium, radium, and

25   thorium at 1460 kev, 1765 kev, and 2614 kev.

26

27   The difference appears to be related most strongly to the efficiency. The efficiency determined from the

28   two calibrations is shown in Table 4-9.

29

30   Table 4-9 shows that the lowest energy was affected the most. This could indicate some additional

31   shielding was somehow placed between the detector and the source during the pad calibration. The point

32   calibration was performed on the detector with it installed in its protective housing but not on the vehicle.

33   The pad calibration, on the other hand, was performed with the entire vehicle setting on the calibration

34   pad. This situation implies that any shielding caused by the vehicle itself would be accounted for only in

1   the pad calibration. The Gator has a large mounting plate below and behind the detector. The plate is

2   approximately 1/8-inch steel and is bolted to another plate of approximately 1/8-inch steel. This would

3   represent a significant portion of the field of view. In addition, the efficiency obtained from the point

4   source calibration matched more closely with the other instruments, while the activity values calculated

5   using these efficiencies did not match other instruments. This implies the efficiency obtained from the

6   point calibration was correct for the detector but not when it was installed on the vehicle. In other words,

7   the vehicle was affecting the calibration. Since there appeared to be such a difference between these two

8   calibrations, any further comparison would have been counterproductive and will not be performed here.

9

10   Again, as with the other detectors, some field data has been analyzed and plotted on graphs. These graphs

11   are shown below.

12
13

Gator Th-232
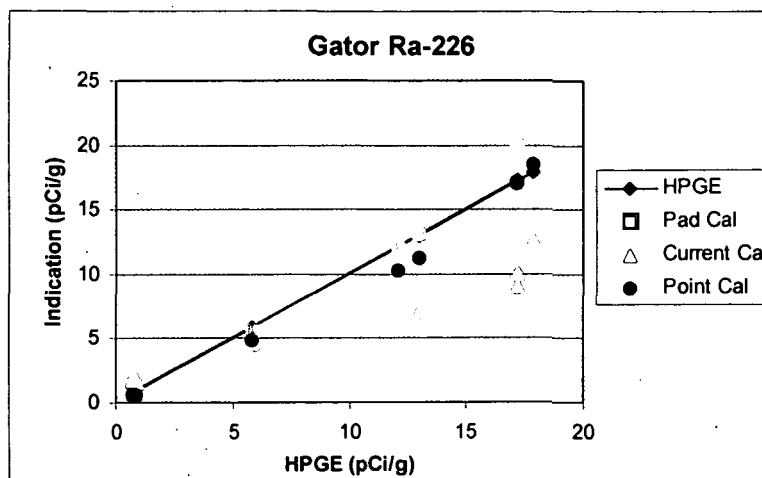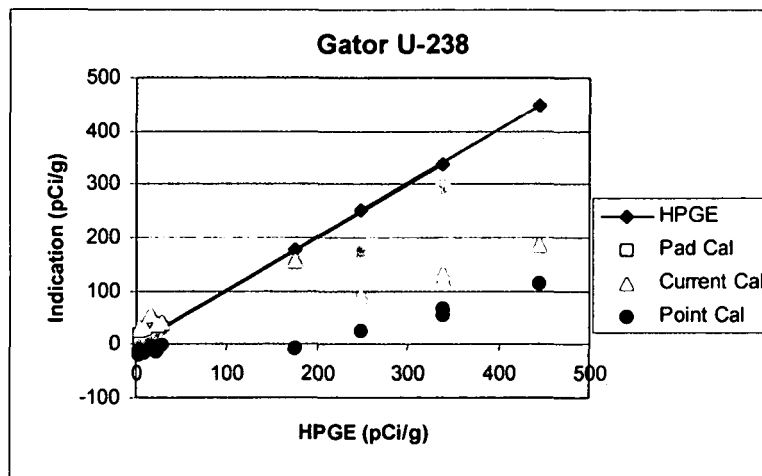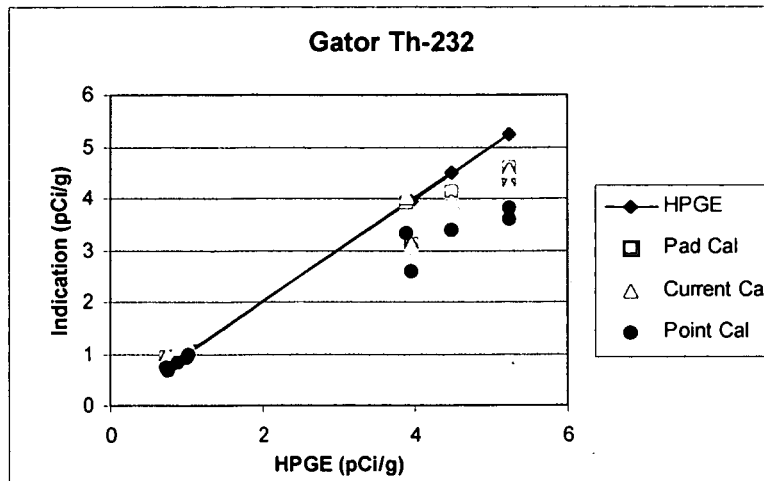
1
2   The plots indicate some outliers in these data. There were significant errors in the uranium coefficients
3   produced by the point source calibration, but the pad calibration accounts for this very well. In addition,
4   the pad calibration out performs the current calibrations in almost every instance.

TABLE 4-1
RSS1 CALIBRATION COEFFICIENT COMPARISON

	Point Source Cal			Pad Calibration			Difference		
F1	4.088	±	0.101	3.767	±	0.109	0.320	±	0.148
F2	0.533	±	0.079	0.633	±	0.077	0.100	±	0.111
F3	-0.431	±	0.158	-0.021	±	0.100	0.410	±	0.186
F4	-0.013	±	0.002	-0.014	±	0.003	0.001	±	0.004
F5	0.131	±	0.007	0.130	±	0.004	0.001	±	0.008
F6	0.066	±	0.007	0.068	±	0.005	0.002	±	0.009
F7	0.000	±	0.000	-0.001	±	0.001	0.000	±	0.001
F8	0.001	±	0.001	0.003	±	0.001	0.001	±	0.001
F9	0.071	±	0.003	0.077	±	0.002	0.006	±	0.004
F10	0.192	±	0.008	0.193	±	0.006	0.001	±	0.010
F11	-0.003	±	0.004	0.001	±	0.007	0.003	±	0.007
F12	-0.055	±	0.008	-0.058	±	0.007	0.003	±	0.010
F13	0.036	±	0.007	-0.005	±	0.006	0.042	±	0.009

TABLE 4-2
RSS1 CALCULATED VALUE FOR PAD CALIBRATION SPECTRA

Values for	Sources used	Theory	HPGe	Point Cal	Pad Cal
Uranium	Uranium	326.5	331	348.40	325.20
	Radium	0	N/D	-25.90	-1.30
	Thorium	0	N/D	-43.50	-1.30
	Background	0	N/D	-4.26	-1.30
Radium	Uranium	0	0.66	0.50	0.38
	Radium	20.37	19.10	20.84	20.75
	Thorium	0	0.73	0.09	0.38
	Background	0	0.51	0.37	0.38
Thorium	Uranium	0	0.56	0.53	0.56
	Radium	0	0.49	0.35	0.56
	Thorium	9.045	8.78	8.94	9.61
	Background	0	0.45	0.52	0.56
Potassium	Uranium	8.28	8.31	8.33	8.29
	Radium	8.28	8.41	8.88	8.29
	Thorium	8.28	8.99	13.29	8.29
	Background	8.28	8.28	8.55	8.29

N/D = none detected

TABLE 4-3
RSS2 CALIBRATION COEFFICIENT COMPARISON

	Point Source Cal	Pad Calibration	Difference
F1	3.849 ± 0.359	4.602 ± 0.163	-0.753 ± 0.394
F2	-0.174 ± 0.061	-0.331 ± 0.074	0.157 ± 0.097
F3	-1.971 ± 0.233	-2.054 ± 0.143	0.083 ± 0.272
F4	-0.011 ± 0.004	-0.014 ± 0.003	0.003 ± 0.006
F5	0.112 ± 0.014	0.108 ± 0.003	0.004 ± 0.014
F6	0.057 ± 0.009	0.053 ± 0.004	0.004 ± 0.009
F7	-0.001 ± 0.001	-0.001 ± 0.001	0.000 ± 0.003
F8	-0.001 ± 0.001	-0.001 ± 0.001	0.000 ± 0.000
F9	0.070 ± 0.011	0.075 ± 0.002	-0.005 ± 0.012
F10	0.166 ± 0.018	0.204 ± 0.007	-0.038 ± 0.020
F11	0.000 ± 0.006	-0.010 ± 0.007	0.01 ± 0.010
F12	-0.038 ± 0.007	-0.027 ± 0.006	-0.011 ± 0.008
F13	0.018 ± 0.006	0.023 ± 0.005	-0.005 ± 0.008

TABLE 4-4
RSS2 CALCULATED VALUES FOR PAD CALIBRATION SPECTRA

Values for	Sources used	Theory	HPGe	Point Cal	Pad Cal
Uranium	Uranium	326.5	331	262.18	315.13
	Radium	0	N/D	7.04	-11.37
	Thorium	0	N/D	-47.15	-11.37
	Background	0	N/D	-11.41	-11.37
Radium	Uranium	0	0.66	0.54	0.27
	Radium	20.37	19.10	21.51	20.64
	Thorium	0	0.73	0.66	0.27
	Background	0	0.51	0.29	0.27
Thorium	Uranium	0	0.56	0.53	0.54
	Radium	0	0.49	0.61	0.54
	Thorium	9.045	8.78	8.93	9.58
	Background	0	0.45	0.50	0.54
Potassium	Uranium	8.28	8.31	7.30	8.46
	Radium	8.28	8.41	3.93	8.46
	Thorium	8.28	8.99	8.11	8.46
	Background	8.28	8.28	6.91	8.46

N/D = none detected

TABLE 4-5
RTRAK CALIBRATION COEFFICIENT COMPARISON

	Point Source Cal	Pad Calibration	Difference
F1	4.093 ± 0.433	5.311 ± 0.204	-1.218 ± 0.478
F2	-0.128 ± 0.100	-0.175 ± 0.093	0.047 ± 0.137
F3	-2.371 ± 0.342	-2.243 ± 0.172	-0.129 ± 0.383
F4	-0.073 ± 0.015	-0.011 ± 0.004	-0.062 ± 0.015
F5	0.138 ± 0.018	0.124 ± 0.003	0.014 ± 0.018
F6	0.108 ± 0.018	0.060 ± 0.005	0.048 ± 0.019
F7	0.001 ± 0.003	-0.001 ± 0.001	0.001 ± 0.003
F8	0.000 ± 0.001	0.000 ± 0.001	0.000 ± 0.001
F9	0.079 ± 0.013	0.083 ± 0.002	-0.004 ± 0.013
F10	0.209 ± 0.024	0.222 ± 0.008	-0.013 ± 0.026
F11	0.030 ± 0.017	-0.009 ± 0.011	0.040 ± 0.020
F12	-0.022 ± 0.015	-0.026 ± 0.007	0.004 ± 0.016
F13	0.002 ± 0.011	0.024 ± 0.007	-0.022 ± 0.013

TABLE 4-6
RTRAK CALCULATED VALUES FOR PAD CALIBRATION SPECTRA

Values for	Sources used	Theory	HPGe	Point Cal	Pad Cal
Uranium	Uranium	326.5	331	243.84	322.03
	Radium	0	N/D	-6.64	-4.5
	Thorium	0	N/D	-77.69	-4.5
	Background	0	N/D	-7.47	-4.5
Radium	Uranium	0	0.66	-3.11	0.45
	Radium	20.37	19.10	23.06	20.82
	Thorium	0	0.73	2.46	0.45
	Background	0	0.51	0.65	0.45
Thorium	Uranium	0	0.56	0.58	0.52
	Radium	0	0.49	0.52	0.52
	Thorium	9.045	8.78	9.17	9.57
	Background	0	0.45	0.50	0.52
Potassium	Uranium	8.28	8.31	10.24	8.40
	Radium	8.28	8.41	8.50	8.40
	Thorium	8.28	8.99	7.13	8.40
	Background	8.28	8.28	7.83	8.40

N/D = none detected

000030

TABLE 4-7
GATOR CALIBRATION COEFFICIENT COMPARISON

	Point source Cal	Pad Calibration	Difference
F1	4.508 ± 0.742	9.185 ± 0.593	-4.677 ± 0.949
F2	0.017 ± 0.092	-0.172 ± 0.186	0.189 ± 0.208
F3	-2.809 ± 0.510	-1.184 ± 0.270	-1.625 ± 0.577
F4	-0.018 ± 0.008	-0.022 ± 0.009	0.004 ± 0.011
F5	0.128 ± 0.028	0.150 ± 0.005	-0.022 ± 0.028
F6	0.055 ± 0.014	0.066 ± 0.006	-0.011 ± 0.015
F7	-0.002 ± 0.002	-0.003 ± 0.003	0.001 ± 0.003
F8	0.003 ± 0.001	0.005 ± 0.001	-0.002 ± 0.003
F9	0.081 ± 0.023	0.092 ± 0.002	-0.011 ± 0.024
F10	0.175 ± 0.033	0.273 ± 0.013	-0.098 ± 0.036
F11	-0.004 ± 0.011	-0.025 ± 0.024	0.021 ± 0.026
F12	-0.029 ± 0.009	-0.020 ± 0.011	-0.009 ± 0.013
F13	0.022 ± 0.008	0.005 ± 0.009	0.017 ± 0.013

TABLE 4-8
GATOR CALCULATED VALUES FOR PAD CALIBRATION SPECTRA

Values for	Sources used	Theory	HPGE	Point Cal	Pad Cal
Uranium	Uranium	326.5	331	150.62	334.53
	Radium	0	N/D	23.37	8.03
	Thorium	0	N/D	-238.29	8.03
	Background	0	N/D	-8.61	8.03
Radium	Uranium	0	0.66	0.27	0.26
	Radium	20.37	19.10	17.63	20.63
	Thorium	0	0.73	0.15	0.26
	Background	0	0.51	0.22	0.26
Thorium	Uranium	0	0.56	0.45	0.51
	Radium	0	0.49	0.17	0.51
	Thorium	9.045	8.78	8.51	9.55
	Background	0	0.45	0.45	0.51
Potassium	Uranium	8.28	8.31	5.82	8.28
	Radium	8.28	8.41	3.05	8.28
	Thorium	8.28	8.99	8.17	8.28
	Background	8.28	8.28	5.45	8.28

N/D = none detected

TABLE 4-9
GATOR CALCULATED EFFICIENCIES

Isotope	Energy (kev)	Pad Calibration Efficiency	Point Source Calibration Efficiency
Uranium	1001	0.109	0.224
Potassium	1460	3.668	5.705
Radium	1765	6.863	7.908
Thorium	2614	11.184	12.681

5.0 RECOMMENDATIONS

5.1 PAD CALIBRATION

The calibration pad should be used for all future NaI detector calibrations at the FEMP. Use of the calibration pad avoids the problems associated with field calibrations of the detectors. The calibration quality using the pad is much improved over the field method since it provides better results than point source calibration and is a more straightforward process.

5.2 ESTABLISHMENT OF A PROCEDURE FOR FUTURE CALIBRATIONS

Future calibrations of the NaI detectors should be performed annually or as needed after major maintenance or modification. It is recommended that such a procedure be established and documented for carrying out such calibrations.

5.3 POINT SOURCE CALIBRATION

The point source calibration method is a viable calibration process with some refinements. There were a few difficulties encountered during the development of this calibration method. The first was the determination of the interference coefficients, which required a strong point source. In order to make a real source behave as a point source, it was necessary to move is a distance away from the detector. The size of the source and the size of the detector dictate the minimum distance. However, as the distance increased, additional source material was required in order to meet the strong source requirement. Some improvements could be made on this situation through experimentation on nominal count times versus source size and distance. It may also be possible to determine some adjustments to the theory based on a planer source rather than a point source.

The second area for improvement is the number of required counts. The procedure discussed in this report required 26 separate counts to be acquired and analyzed. A rotating calibration jig could allow the detector to rotate while the source is held stationary. This improvement would reduce the number of counts from 26 to 11 and greatly reduce the calculations required to perform the calibration.

Since the calibration pad has emerged as the superior calibration process, it is not recommended that these improvements be pursued at this time. Even with these improvements, the point source calibration process will be less direct and more cumbersome. It is, however, a much quicker and simpler process to set up initially. This process should be considered as a viable option for any future instrumentation or situations that the existing calibration pad can not account for.

1 ## 5.2 REDESIGN GATOR DETECTOR MOUNT

2 As discussed in Section 4.5, the detector mount on the Gator acts as a significant shield to the detector.

3 Such shielding was not intended. While calibration using the pad provides accurate calibration

4 coefficients, the detector's field of view and the system's sensitivity are affected. It is recommended that

5 the mount be redesigned and the Gator's detector recalibrated before the system is used in the field.

000034

6.0 CONCLUSIONS

1

2

3 The theoretical values for the calibration pad were determined purely from theory and from laboratory

4 measurements of the sources. The agreement between these theoretical values and the HPGe

5 measurements obtained on the calibration pad prove that this process is accurate.

6

7 The Pad Calibration process is an improvement on the current process, as indicated in nearly every case

8 from the plots in Section 4. The plots included some locations that were not included in the original

9 calibration on several of the instruments. Some of these points were thrown out as outliers during the

10 original calibration but showed a reasonable match when this calibration was applied.

11

12 Also, since this method represents a sealed source calibration, the calibration points are not in danger of

13 being lost to remediation activities. This represents a significant improvement in real-time instrument

14 methodology because the gamma ray flux can be re-established and calibrations can be repeated at a fixed

15 frequency.

16

17 The new ROIs chosen for this calibration appear to be an improvement. While a detailed analysis of this

18 has not been performed, the coefficients obtained from this calibration (using new ROIs) indicate, in most

19 cases, a much smaller dependence on interference isotopes than the original calibration. This implies the

20 activity calculated from using these ROIs will be a more direct measurement then if the original ROIs are

21 used.

22

3317

REFERENCES

David Allen, 1999, "Direct Calibration of NaI detectors using Calibration Pad."

H. L. Beck, J. DeCampo, C. Gogolak, 1972, "*In Situ* Ge(Li) And NaI(Tl) Gamma-Ray Spectrometry," USAEC Report HASL-258.

Thomas Cox, 1999, "Measurement Symmetry Test for Sodium Iodide Detectors."

Anthony Foderaro, 1976, "The Photon Shielding Manual," Pennsylvania State University.

Kevin Miller, Peter Shebell, 1993, "*In Situ* Gamma-Ray Spectrometry: A Tutorial for Environmental Radiation Scientists," EML-557, DOE-Headquarters.

U.S. Department of Energy, 1999, "RTRAK Applicability Study," Revision 2, DOE, Fernald Environmental Management Project, Cincinnati, OH.

APPENDIX A

DIRECT CALIBRATION OF NAI DETECTORS USING A CALIBRATION PAD

APPENDIX A
DIRECT CALIBRATION OF NAI DETECTORS USING A CALIBRATION PAD

A.1 SUMMARY

The concept behind direct calibration of the NaI instruments was to count a source of known concentration to determine the detector response using the same geometry that will be present in field counts. The practical aspects of this idea caused the process to be performed with conditions different than would be encountered in the field. This appendix addresses the specific details there were required for the calibration process, including the adjustments made to account for less than ideal conditions. A list of variables and a summary of the equations related to this calibration are included in this appendix. This allows the equations to be presented in as concise an array as possible by allowing several equations to be derived for only one example.

A.2 NaI CALIBRATION EQUATIONS

The goal of the calibration was to determine efficiency and interference coefficients to be used during field counting. The efficiency is simply a ratio of the net count rate detected and the activity concentration of a known source. The NaI detectors are designed to be calibrated to an infinitely large, homogeneously distributed source. Since an infinitely large source is not practical, the source pattern on the calibration pad only produced a portion of the expected homogeneous flux. This meant that the known activity concentrations of the sources would have to be reduced by that portion so an accurate efficiency could be determined. Mathematically the activity is expressed as:

$$Eff = net\ rate/(f*conc.)$$

<div align="right">Equation A-1</div>

Where f is the fraction of the infinite source actually represented by the source pattern. The calculations used to derive these values are included in Appendix B. Once determined, the efficiency was used to divide the corrected net count rate of an isotope in order to obtain the activity concentration of interest. The corrected net counts were the net counts corrected for any interference caused by other isotopes. The equations for the corrected net counts are:

$$U_{cnet} = U_{net} - k1*Ra_{cnet} - k2*Th_{cnet}$$
$$Ra_{cnet} = Ra_{net} - k3*U_{cnet} - k4*Th_{cnet}$$
$$Th_{cnet} = Th_{net} - k5*U_{cnet} - k6*Ra_{cnet}$$

<div align="right">Equation A-2</div>

Where the "cnet" subscript represents corrected net counts and the "net" subscript represents raw net counts. The "k" factors are the interference coefficients. Where there are no interfering counts, the above

000038

1   equation simply states that the raw net counts are the corrected net counts. In addition, the interference

2   coefficients are multiplied by the corrected net counts, not the raw net counts. This was necessary since

3   the raw net counts were influenced by interference of their own, while the interference coefficient

4   depended on (and was determined by) using interference-free spectra.

5

6   The interference coefficients were determined by loading the interfering isotope into the calibration pad,

7   in the specified pattern, and acquiring a spectrum. Once the spectrum was acquired, the net counts for all

8   the isotopes of interest were determined. Then a ratio was made of the net counts in the region of the

9   interfering isotope and the net counts in the region of the isotope of interest. For example, the

10   interference coefficient for uranium-238 from radium-226 (k1 above) was determined by first counting the

11   radium-226 sources in the calibration pad and then dividing the uranium-238 net counts by the

12   radium-226 net counts. Since only radium-226 sources were in the pad, the corrected radium-226 net

13   counts were equal to the raw net counts, and the uranium-238 and thorium-232 corrected net counts were

14   equal to zero. This process was repeated for each isotope of interest. The radium-226 net counts obtained

15   when the radium-226 sources were counted were used to determine the radium-226 efficiency as

16   described above. In this manner, only one spectrum from each isotope was required for the calibration.

17

18   The equations above indicate that, when field counting is performed, the uranium-238 corrected net

19   counts can not be determined until the radium-226 corrected net counts are determined. But the

20   radium-226 corrected net counts can not be determined until the uranium-238 corrected net counts are

21   determined. However, when field counting a spectrum, the raw net counts and the interference

22   coefficients will already be known. As a result, there are three equations and three unknowns, meaning

23   that the equations can be solved simultaneously. The solutions to the above equations are:

24

25 $$Ucnet = \frac{(1 - k4 \cdot k6) \cdot Unet + (k2 \cdot k6 - k1) \cdot Ranet + (k1 \cdot k4 - k2) \cdot Thnet}{(1 - k3 \cdot k1 - k5 \cdot k2 + k3 \cdot k2 \cdot k6 + k4 \cdot k5 \cdot k1 - k4 \cdot k6)}$$

26

27 $$Racnet = \frac{(k4 \cdot k5 - k3) \cdot Unet + (1 - k5 \cdot k2) \cdot Ranet + (k3 \cdot k2 - k4) \cdot Thnet}{(1 - k3 \cdot k1 - k5 \cdot k2 + k3 \cdot k2 \cdot k6 + k4 \cdot k5 \cdot k1 - k4 \cdot k6)}$$

28

29 $$Thcnet = \frac{(k6 \cdot k3 - k5) \cdot Unet + (k5 \cdot k1 - k6) \cdot Ranet + (1 - k3 \cdot k1) \cdot Thnet}{(1 - k3 \cdot k1 - k5 \cdot k2 + k3 \cdot k2 \cdot k6 + k4 \cdot k5 \cdot k1 - k4 \cdot k6)}$$

30   Equation A-3

31

1   It is convenient to rewrite these equations at this point as follows:

2

3    $U_{cnet} = F1*U_{net} + F2*Ra_{net} + F3*Th_{net}$

4    $Ra_{cnet} = F4*U_{net} + F5*Ra_{net} + F6*Th_{net}$

5    $Th_{cnet} = F7*U_{net} + F8*Ra_{net} + F9*Th_{net}$

6   Equation A-4

7   where:

8

9    $F1 = (1-k4*k6)/(1-k3*k1-k5*k2+k3*k2*k6+k4*k5*k1-k4*k6)$

10   Equation A-5

11

12   F2, F3, F4, F5, F6, F7, F8, and F9 have similar expressions relating them to the coefficients of the raw net

13   counts of each isotope. The complete equations are included at the end of this appendix. It should be

14   noted at this point that while the "k" values have a physical meaning (interference ratio), the "F" values

15   are purely a mathematical solution to simultaneous equations.

16

17   The "F" values and the efficiency values were, then, the goals of the calibration procedure. As one

18   additional time-saving step, the "F" values were divided by the appropriate efficiency so that the raw net

19   count rates only needed to be multiplied by one factor and summed to obtain the desired results.

20

21   A.3 <u>CORRECTING FOR NATURAL ISOTOPES IN THE PAD MATERIAL</u>

22   It is important to note at this point that the calibration pad itself had some small amount of naturally

23   occurring isotopes. However, the equations for the interference coefficients require an interference-free

24   spectrum. In addition, the efficiency equation required determining the detectors' response to a known

25   source. In order to obtain a spectrum that represents only the sources, it was necessary to collect an

26   ambient background spectrum. The counts from each region of this spectrum were then subtracted from

27   the counts in the identical regions of the source spectra. The results were interference-free spectra

28   acquired from a known source.

29

30   A.4 <u>SPECTRUM ACQUISITION</u>

31   The calibration pad used a source pattern that consists of 45 sources arranged in a circular pattern. The

32   area represented by each source, as well as the source activity, is held constant. This allowed for an easy

33   to understand average concentration for the entire pad. A detailed calculation was performed in order to

34   ensure that the shape of the flux represented a homogeneous environment and to determine the fraction of

35   an infinite source that was accounted for. The details of this calculation are included in Appendix B.

36

1   The detector was placed at the center of the pattern and spectra were acquired for 5 minutes each. A total

2   of four spectra were acquired, one ambient background spectrum plus one with each type of source

3   loaded into the pad. All the spectra required to calibrate an instrument were acquired in the same

4   afternoon.

5   A.5 SPECTRUM ANALYSIS

6   Once all the spectra were acquired, the counts from the ambient background spectrum were subtracted

7   from the counts obtained from the source spectra. The exact same ROIs that will be used for field

8   counting were used to determine the counts in all the regions of the spectra, including background

9   regions. The net counts for all the isotopes are then determined using the following equation:

10

11   $Net = C_{ROI} - N_{ROI}/N_{Bkg} * C_{Bkg}$

12   Equation A-6

13

14   where

15

16   C_{ROI} = the total counts in the isotope region
17   C_{Bkg} = the total counts in both background regions associated with the ROI above
18   N_{ROI} = the number of channels in the ROI above
19   N_{Bkg} = the number of channels in both background regions associated with the ROI above

20

21   The net counts were then used to determine the efficiency and interference coefficients as described

22   earlier. For example, the net counts determined from the radium-226 spectrum were used as follows:

23

24   $Eff_{Ra} = Ranet /(LT * f * conc._{Ra})$

25   Equation A-1

26   and

27

28   $k1 = Unet/Ranet$ and $k6 = Thnet /Ranet$

29   Equation A-7

30

31   where:

32

33   Eff_{Ra} = the efficiency of the detector for Ra-226 (cps/pCi/gm)
34   Unet   = the net counts in the U-238 ROI (Th and Ra have the same meaning for the respective
35   isotopes)
36   f   = the fraction of an infinite source actually represented by the source pattern
37       $conc._{Ra}$ = the Ra-226 activity concentration of the calibration pad
38   LT   = live time in seconds

39

40   Once all the "k" values are determined, these values are used to determine the "F" values mentioned

41   earlier. This process is then repeated for each isotope.

42

000041

1 A.6 POTASSIUM-40

2 Currently the activity of potassium-40 is determined as part of the spectrum analysis. There is no

3 regulatory purpose for this, but it provides a valuable resource for quality assurance. Since potassium-40

4 has no regulatory purpose, no potassium-40 sources were purchased or manufactured. Instead it was

5 deemed acceptable to use the small amount of potassium-40 in the material the pad was constructed with.

6 This was accomplished by using an HPGe detector to characterize the amount of potassium-40 in the pad.

7 Once this was done, the efficiency was calculated by first determining the potassium-40 net count rate,

8 obtained from the ambient background spectrum, and then dividing this by the potassium-40 activity

9 determined by the HPGe. This was similar to Equation 1 used for the other isotopes except "f" (the

10 fraction of the infinite flux represented by the pattern) was equal to one. The other difference was no

11 ambient background spectrum is subtracted from this one. Obviously, if the ambient background is

12 subtracted, no potassium-40 counts would exist to determine the efficiency. Therefore, any interference

13 from other isotopes in the pad material would have affected the value obtained for the potassium-40

14 efficiency. The amount of other isotopes was small, however, and an estimate of the true value could be

15 obtained once the potassium-40 interference coefficients were determined. Once the calibration was

16 finished, this estimate revealed an insignificant difference.

17

18 The interference coefficients for potassium-40 were also determined in a similar manner to the other

19 isotopes. However, there were a few differences due to the nature of potassium-40. First, it is important

20 to note that there was no interference from potassium-40 on any of the isotopes of concern, so there was

21 no need to determine an interference factor from potassium-40. There was, however, a need to determine

22 the interference from the other isotopes on potassium-40. This was easily done with the source spectra

23 obtained as part of the calibration. Since net counts appearing in the potassium-40 region were affected

24 by three other isotopes as well as by potassium-40 itself, it was necessary for an equation describing this

25 to have four terms. In keeping with equation 2, this equation becomes:

26

27 $K_{cnet} = K_{net} - k7 * U_{cnet} - k8 * Ra_{cnet} - k9 * Th_{cnet}$

28   Equation A-8

29

30 As before, the "cnet" subscript represents corrected net counts and the "net" subscript represents raw net

31 counts.

32

33 These "k" factors were determined in the same manner as they were for the other isotopes. Since the

34 ambient background spectrum was subtracted from the source spectrum, the only influence on the

35 resultant spectrum was from the source that was loaded into the calibration pad. This meant that the

1   corrected net potassium-40 counts, as well as the corrected net counts from the other isotopes, was zero.

2   That left only the potassium-40 raw net counts and the corrected net counts of the isotope loaded into the

3   pad. With equation 8 reduced to only two terms, it was simple to solve the remaining portion for the

4   appropriate "k" factor. In this manner, each of the above "k" factors were determined, one for each

5   source loaded into the pad.

6

7   This would be an appropriate stopping point for the calibration process. In the field, the corrected net

8   count rate of each isotope could be determined and then multiplied by the appropriate "k" factor to correct

9   the raw K-40 net counts for interference. However, it would be necessary to determine coefficients for

10   the raw net count rate for the other isotopes; therefore, it would not be necessary to determine the

11   corrected net count rate for these isotopes in the field. It would be easier if these coefficients could be

12   converted to coefficients for the raw net counts rate rather than the corrected net count rate of the other

13   isotopes. This would be done by starting with equations listed as equation 4 and inserting them into

14   equation 8 above:

15

16 $K_{cnet} = K_{net} - k7*\{F1*U_{net} + F2*Ra_{net} + F3*Th_{net}\} - k8*\{F4*U_{net} + F5*Ra_{net} + F6*Th_{net}\} - k9*\{F7*U_{net} +$

17 $F8*Ra_{net} + F9*Th_{net}\}$

18   Equation A-9

19

20 Rearranging, we get:

21

22 $K_{cnet} = K_{net} + \{-k7*F1 - k8*F4 - k9*F7\}*U_{net} + \{-k7*F2 - k8*F5 - k9*F8\}*Ra_{net} + \{-k7*F3 - k8*F6 - k9*F9\}*$

23 Th_{net}

24

25   Equation A-10

26

27 All the terms in brackets are multipliers (coefficients) of the raw net count rates of the other isotopes.

28 These coefficients were designated as F11 through F13 in the order they appear above. F10 is an

29 imaginary coefficient for the raw potassium-40 net count rate and has the value of one since these values

30 will be divided by the potassium-40 efficiency before they are used in the field. Having a value for F10

31 simply keeps this process clear by avoiding the confusion of one additional term. The values are divided

32 by the efficiency simply to avoid performing this process for each and every field spectrum collected.

1 A.7 SUMMARY OF EQUATIONS

2 This attachment provides a summary of all the equations associated with the direct calibration of the NaI

3 instruments.

4

5 A.7.1 Efficiency

6 The efficiency is determined by Equation 1 in the text.

7

8 Eff=net rate/(f*conc.)

9

10 where:

11

12 Net rate = Net/LT {net is the net counts for the isotope loaded into the calibration pad}

13

14 Conc. = Act/(area*15*ρ) {where the area is 3292 cm^2, the density of the pad (1.6 g/cc), and act is the

15 average activity of each source}

16

17 and f is determined mathematically for the given source pattern and gamma energy. For the circular

18 pattern with 45 sources, the values for f are given in the table below.

19

20 **PAD GAMMA FLUX CALCULATION PARAMETERS**

21

Energy (kev)	Mass attenuation coefficient for air (cm^2/gm) $(\mu/\rho)_a$	Mass attenuation coefficient for air (cm^2/gm) $(\mu/\rho)_s$	Ratio of discrete flux averaged over the detector area to the homogeneous flux (f)
1001	0.0636	0.0635	0.7807
1765	0.0475	0.0477	0.7304
2614	0.0385	0.0393	0.6874

22

23 These are calculated using values of 1.6 g/cc for soil density, 0.001293 g/cc for air density, 31 cm for the

24 detector height, and 15cm for the length of the sources.

25

26 **Corrected Net Counts**

27 The equations for the corrected net counts are:

28

29 $U_{cnet} = F1*U_{net} + F2*Ra_{net} + F3*Th_{net}$

30 $Ra_{cnet} = F4*U_{net} + F5*Ra_{net} + F6*Th_{net}$

31 $Th_{cnet} = F7*U_{net} + F8*Ra_{net} + F9*Th_{net}$

32 $K_{cnet} = F10*K_{net} + F11*U_{net} + F12*Ra_{net} + F13*Th_{net}$

33

1   where:

2

3    $F1 = (1-k4*k6)/(1-k3*k1-k5*k2+k3*k2*k6+k4*k5*k1-k4*k6)$

4    $F2 = (k2*k6-1)/(1-k3*k1-k5*k2+k3*k2*k6+k4*k5*k1-k4*k6)$

5    $F3 = (k1*k4-k2)/(1-k3*k1-k5*k2+k3*k2*k6+k4*k5*k1-k4*k6)$

6    $F4 = (k4*k5-k3)/(1-k3*k1-k5*k2+k3*k2*k6+k4*k5*k1-k4*k6)$

7    $F5 = (1-k5*k2)/(1-k3*k1-k5*k2+k3*k2*k6+k4*k5*k1-k4*k6)$

8    $F6 = (k3*k2-k4)/(1-k3*k1-k5*k2+k3*k2*k6+k4*k5*k1-k4*k6)$

9    $F7 = (k6*k3-k5)/(1-k3*k1-k5*k2+k3*k2*k6+k4*k5*k1-k4*k6)$

10   $F8 = (k5*k1-k6)/(1-k3*k1-k5*k2+k3*k2*k6+k4*k5*k1-k4*k6)$

11   $F9 = (1-k3*k1)/(1-k3*k1-k5*k2+k3*k2*k6+k4*k5*k1-k4*k6)$

12   $F10 = 1$

13   $F11 = -k7*F1-k8*F4-k9*F7$

14   $F12 = -k7*F2-k8*F5-k9*F8$

15   $F13 = -k7*F3-k8*F6-k9*F9$

16

17   and

18

19   $k1=U_{net}/Ra_{net}$, $k6 = Th_{net}/Ra_{net}$, and $k8 = K_{net}/Ra_{net}$ {determined with Ra-226 sources loaded into the
20   calibration pad}

21

22   $k2=U_{net}/Th_{net}$, $k4 = Ra_{net}/Th_{net}$, and $k9 = K_{net}/Th_{net}$ {determined with Th-232 sources loaded into the
23   calibration pad}

24

25   $k3=Ra_{net}/U_{net}$, $k5 = Th_{net}/U_{net}$, and $k7 = K_{net}/U_{net}$ {determined with U-238 sources loaded into the
26   calibration pad}

27

28   ## A.8 DEFINITION OF VARIABLES

29   Most variables appearing in this document follow this format. Occasionally some additional subscripts

30   have been added in the text to better clarify a point.

31

32	Act.	The activity of a source expressed in pCi (or grams if ppm is desired)
33	C_{Bkg}	Total counts in the background region of a spectrum (counts)
34	C_{ROI}	Total counts in the isotope region of a spectrum (counts)
35	Conc.	Activity concentration of the calibration pad (pCi/gm or ppm)
36	Eff	The efficiency of a detector for a particular isotope
37	f	The fraction of the expected homogeneous flux presented by a pattern of sources
38	Fi	A coefficient to be multiplied by raw net counts in order to obtain corrected net counts
39	K_{cnet}	The corrected net counts from the Postasium-40 (K-40) region of a spectrum (counts)
40	ki	The interference coefficient for a given isotope interfering with another specific isotope
41	K_{net}	The raw net counts from the Postasium-40 (K-40) region of a spectrum (counts)
42	LT	Spectrum live time (sec)
43	N_{ROI}	The number of channels in the isotope ROI for the isotope of interest (channels)
44	N_{Bkg}	The number of channels in the background ROI for the isotope of interest (channels)
45	net	The net counts from a generic isotope (counts)
46	net rate	The net counts from a generic isotope divided by the spectrums live time (counts per sec.)
47	Ra_{cnet}	The corrected net counts from the Radium-226 region of a spectrum (counts)
48	Ra_{net}	The raw net counts from the Radium-226 region of a spectrum (counts)

1	Th_{cnet}	The corrected net counts from the Thorium-232 region of a spectrum (counts)
2	Th_{net}	The raw net counts from the radium Thorium-232 of a spectrum (counts)
3	U_{cnet}	The corrected net counts from the Uranium-238 region of a spectrum (counts)
4	U_{net}	The raw net counts from the Uranium-238 region of a spectrum (counts)
5	ρ	Rho, a symbol representing the density of a material (g/cc)

APPENDIX B

DISTRIBUTION OF DISCRETE SOURCES
TO SIMULATE A HOMOGENOUS ENVIRONMENT

APPENDIX B
DISTRIBUTION OF DISCRETE SOURCES
TO SIMULATE A HOMOGENOUS ENVIRONMENT

B.1 INTRODUCTION

Calibrating any radiation detector is ideally performed using a known source in the same geometry and conditions as the samples to be analyzed. In keeping with this principle, the NaI detectors would be calibrated using and infinitely large, homogeneously distributed source of known activity with a matrix that resembles soil. Since this is not practical, one alternative is to *simulate* the homogeneous environment with numerous discrete sources.

A detailed analysis was initially prepared analyzing various types of patterns, including the number of sources to be used in each pattern as well as the strength of the sources. That analysis was then used to decide upon the pattern that was eventually used in the calibration pad as well as the strength of the manufactured sources. This appendix describes the theory in detail as well as showing the results of some of the calculations. Some of these results contain information related to other patterns that were part of the analysis. Since the purpose of this appendix is to describe the pattern that was actually used, the details of these additional patterns, as well as the analysis related to them, will not be discussed here.

B.2 THE HOMOGENEOUS ENVIROMENT

The gamma ray flux emitted from an infinitely large homogeneous environment can be determined using the following equation:

$$\phi = \frac{Sv \cdot \left(\frac{\mu a}{\rho a}\right) \cdot \rho a \cdot h}{\rho s \cdot 2 \cdot \left(\frac{\mu s}{\rho s}\right)} \cdot \left[\frac{e^{-\frac{\mu a}{\rho a} \cdot \rho a \cdot h}}{\left(\frac{\mu a}{\rho a}\right) \cdot \rho a \cdot h} - E1\left[\left(\frac{\mu a}{\rho a}\right) \cdot \rho a \cdot h \right] \right]$$

Equation B-1

where:

ϕ = The number of gamma rays per square centimeter per sec arriving at the detector

Sv = The number of gamma rays per sec per cubic centimeter of soil emitted by the soil

μ/ρ = The mass attenuation coefficient, the subscripts represent air (a) and soil (s)

ρ = The density of a substance in gm/cc, again the subscripts represent air and soil.

h = The detector height above the ground

$E_1(x)$ = The exponential integral function (this function is tabulated in a number of text).

The exponential integral function can be approximated for values of x <0.1 by $E_1(x)=\ln(1/x)-0.5772$ with an accuracy of within 1 percent (Reference 2). All the factors except the detector height (h) depend only

1   on the material (soil and air) and the gamma ray energy of interest. Logically, then, the gamma flux in

2   this situation varies only with detector height, not position. As a result, a pattern of discrete sources

3   produce as flat a flux profile as possible over the area the detector is located.

4

5   B.3 THE DISCRETE ENVIRONMENT

6   The sources manufactured for the calibration pad at the FEMP for direct calibration of NaI detectors were

7   cylindrical. The dimensions were a diameter of 1.25 inches and a height of 6 inches. The density of the

8   sources was approximately 1.6 gm/cc. These sources were inserted into the soil of the calibration pad to a

9   depth of 6 inches, making the top of the source level with the surface of the pad.

10

11   As a general rule of thumb, sources behave as point sources when the distance between the source and the

12   point of interest is at least three times the longest dimension of the source. Thus, the sources described

13   above could be approximated as line sources as long as the distance between the source and the point of

14   interest was at least 3.75 inches. The short dimension was used in this case because it was being

15   approximated as a line source not a point source. This approximation provided an infinitely thin line of

16   source material that was 6 inches long.

17

18
19
20
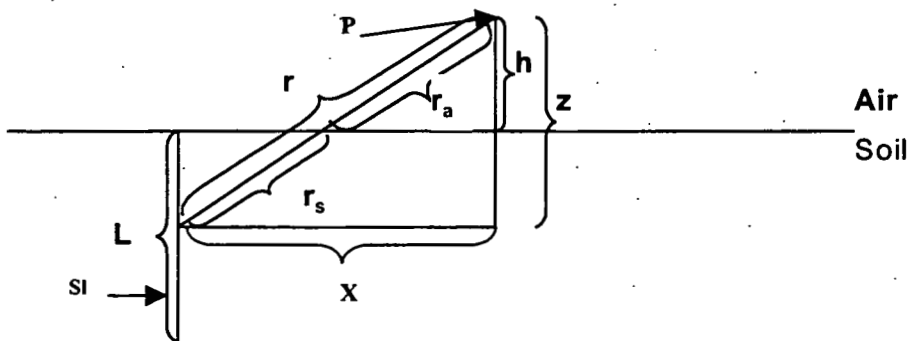
1 The above diagram shows that the gamma flux at the detection point P, from a line source S, can be

2 expressed as:

3

4
$$\phi = \int_{h}^{h+L} \frac{Sl}{4\pi \cdot r^2} \cdot e^{-\frac{\mu s}{\rho s} \cdot \rho s \cdot rs} \cdot e^{-\frac{\mu a}{\rho a} \cdot \rho a \cdot ra} \, dz$$

5
6   Equation B-2
7
8 where:
9
10 Sl = The line source activity (gammas per sec per cm)
11 μ/ρ = The mass attenuation coefficient, the subscripts represent air (a) and soil (s)
12 ρ = The density of a substance in gm/cc, the subscripts represent air and soil.
13 h = The detector height above the ground
14 r = the distance in centimeters depicted on the drawing.
15

16 Integrating the above equation over z from h to h+L yields an equation for the flux from the source at the

17 detection point. The values for r, r_a, and r_s can be rewritten as follows.

18

19 $r = \sqrt{x^2 + z}$

20 $ra = r \cdot \dfrac{h}{z} = \sqrt{x^2 + z^2} \cdot \dfrac{h}{z}$

21 $rs = r - ra = \sqrt{x^2 + z^2} \cdot \left(1 - \dfrac{h}{z}\right)$

22

23 This expression can be solved numerically by dividing z into small increments represented by Δz.

24 Substituting (h+n*Δz) for z, where n is a whole number between 1 and the number of increments that z is

25 divided into, substituting Δz for dz, replacing the integral with a summation, and substituting the above

26 expressions for r, r_a, and r_s allows rearrangement of the variables to obtain the following expression:

$$\Phi = \frac{Sl}{4*\pi} * \sum \left[\frac{1}{X^2 + (h+n*\Delta z)^2} * e^{\sqrt{X^2+(h+n*\Delta z)^2} * \left[\left[\frac{\mu s}{\rho s}*\rho s - \frac{\mu a}{\rho a}*\rho a \right] * \frac{h}{(h+n*\Delta z)} - \frac{\mu s}{\rho s}*\rho s \right]} \right] * \Delta z$$

27
28
29   Equation B-3
30
31 This is easily calculated using a spreadsheet once the detector height (h), the source activity (S_L), and the

32 gamma ray energy are assumed.

1   Once a pattern was selected, the value of X from each source to the detection point could be calculated

2   and the flux determined. All these fluxes could then be summed to determine the flux at that point from

3   all the discrete sources. Next, the volume of soil represented by the sources was determined and the

4   activity of all the sources divided by this volume to obtain the activity concentration. This activity

5   concentration was then inserted into the homogeneous equation (equation 1) and compared to the flux

6   calculated from the pattern of discrete sources.

7

8   B.4 SOURCES

9   Before performing any calculations, the source activity had to be converted into units of gammas/sec/cm

10 for Sl and gammas/sec/cc for Sv. In both cases, the average total activity per source was used. To

11 calculate the value for Sl, this total activity was then multiplied by 0.037 disintegrations per sec/pCi, by

12 the gamma yield (0.00845 gammas/disintegration for uranium-238) and divided by 15cm. This gave

13 values of 689.1, 919.5, and 917.6 gammas/sec/cm for uranium-238, radium-226, and thorium-232

14 respectively.

15

16 Sv was calculated by starting with the total activity per source and dividing it by the volume represented

17 by each source (3292 cm^2 * 15cm). This activity per volume was then multiplied by 0.037 disintegrations

18 per sec/pCi and the gamma yield. This gives values of 0.2093, 0.2793, and 0.2787 gammas/sec/cc for

19 uranium-238, radium-226, and thorium-232 respectively. As long as the area per source is held constant,

20 other patterns can be analyzed with this data by simply adjusting the area per source (3292 cm^2) to the

21 new pattern and recalculating.

22

23 Also required is the real pad concentration averaged over the area of the pattern. This is found by again

24 dividing the total activity per source by the volume represented by each source (3292 cm^2 * 15cm). This

25 product is then divided by the pad density (1.6 g/cc) in order to obtain the activity in units of pCi/g. The

26 values calculated for this are 418.48, 27.75, and 13.08 pCi/g for uranium-238, radium-226, and

27 thorium-232 respectively. Again, analysis of different patterns can use this data by simply adjusting the

28 area per source in this calculation.

29

30 B.5 PATTERN ANALYSIS

31 A circular pattern was chosen for the calibration pad, consisting of one center source with concentric

32 rings moving out from the center. The area per source was held constant. In this way, the pad

33 concentration could be held constant through the pattern by varying the radius or the number of sources

34 per ring. The number of sources in each ring was varied to arrive at a reasonable value for the radius.

1   The sources within a ring were spaced evenly throughout the ring. They were placed at a radius that

2   evenly splits the area of the ring. The values for a 45 source circular pattern with an area per source of

3   3292 cm^2 are shown in the table below.

4
5
6   **CALIBRATION PAD LAYOUT PARAMETERS**
7

Ring Number	Number of Sources in Ring	Radius of Outer Ring	Radius Sources Placed at
1	1	32.4	0
2	4	73.4	56.1
3	8	116.7	97.1
4	8	148.3	133.5
5	8	174.3	161.9
6	8	196.9	186.0
7	8	217.2	207.3

8

9   One of the primary areas of interest in the pattern is how well the pattern represents the homogeneous

10   case of this concentration. To evaluate this, a spreadsheet was developed to perform the numerical

11   integration described earlier for various distances from the detection point (X). A number of detection

12   points, representing the area of the detector, were then picked and the distance from that point to every

13   source in the pattern calculated. From that information, the flux at the detection point from each source

14   could be calculated and summed. Performing this procedure for a number of detection points over the

15   area of the detector can produce the average flux except at the detector. The highest flux was found to be

16   directly over the center of the center most source in the pattern, as expected. Using a 45-source pattern,

17   the flux was evaluated for a variety of areas per source. The chart below shows the comparison of the

18   expected homogeneous flux to the maximum flux of the pattern for the uranium-238 sources. The chart

19   also includes the ratio of the maximum flux to the average flux over the detector area.

20
21   **CALCULATED FLUX PARAMETERS FOR THE CALIBRATION PAD**
22

Area Per Source	Ratio Max Flux to Homogeneous Flux	Ratio Pattern Max Flux to Triangle Center Flux
195	.376	.971
779	.614	1.001
3292	.780	.985
7015	.977	.947
12471	1.327	.926

23

24   The last column shows that as the area per source gets smaller, the ratio in the last column gets closer to

25   one, which implies closer to homogeneous. The 195 cm^2 area data actually was lower than the 779-cm^2

1   area data, possibly because the physical area encompassed by the sources was too small. In other words,

2   45 sources were not sufficient since the area per source was only 195 cm^2. The ratio of maximum flux to

3   homogeneous flux also demonstrated this effect. The 195-cm^2 area data indicated the maximum flux was

4   only 37.6 percent of what would be expected if the source were homogeneous, while the last column

5   indicates that the flux was nearly flat. This was due to the fact that apparently 62.4 percent of the

6   homogeneous flux came from outside the physical boundaries of the pattern. That is, for the 195cm^2 area

7   data, the longest dimension of the pattern is a 52.85-cm radius and apparently, a large amount of the flux

8   for the homogeneous case comes from farther away.

9

10   As the area per source was increased, this ratio became closer to one. This effect can be easily seen in the

11   plot. In this plot, the total area of the pattern, or the product of the area per source and the number of

12   sources, was used.
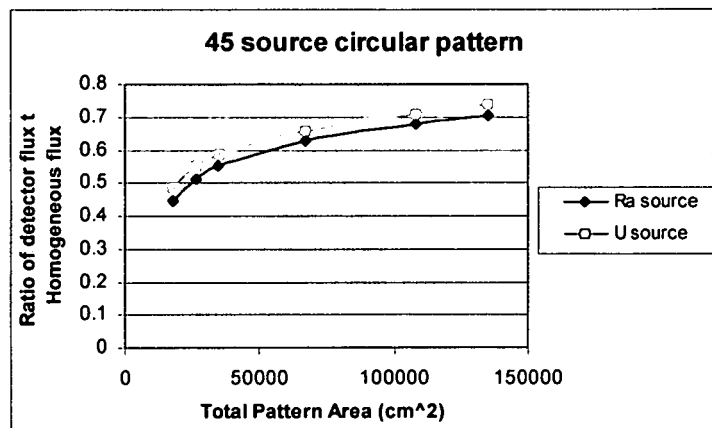
13   The plot shows an increase in the ratio as the overall area of the pattern increases. This at first appeared

14   to be due to the field of view effect, indicating that the larger the pattern, the closer it came to the infinite

15   homogeneous case. Unfortunately there is another effect related to the shape of this plot. With the

16   sources relatively close together, the flux was relatively flat. As the distance between sources increased,

17   the unevenness of the flux became more pronounced, with the highest flux being centered over the center

18   source. This caused the flux in the area covered by the detector to be higher than the average flux in the

19   area represented by the source. This "buckling" of the flux caused the ratio discussed above to increase to

20   values greater than one for sources spaced far apart. The plot below was constructed for a different

21   pattern analyzed but it shows this effect very well.

000053
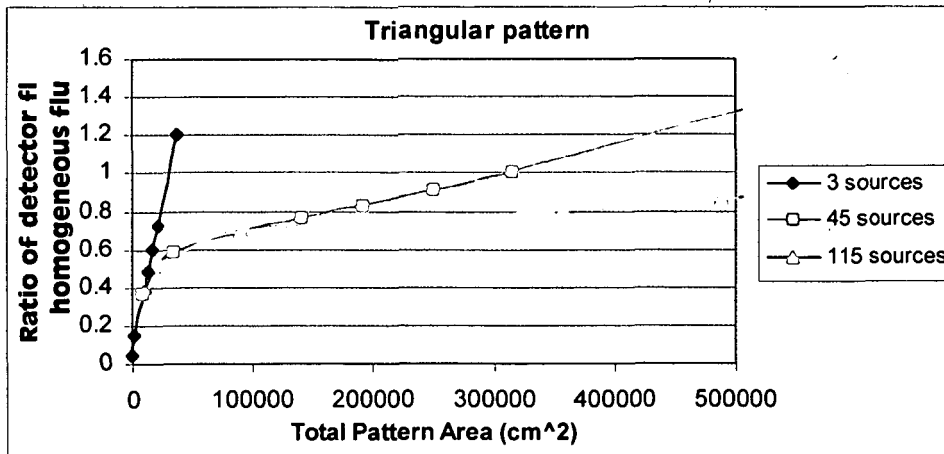
At first it seems possible to locate the point at which the pattern has a ratio of one and simply space the sources that far apart. However, there were other items to consider. First, as the area per source increased, the flatness of the flux began to degrade. In fact, this degradation of the flatness is precisely how a source of a finite area can produce the same flux as a source of infinite area. Second, the point where this ratio reached one was approximately 7015 cm^2. With the 1.25 inch diameter source, this indicates that the sources would cover only about 0.11 percent of the area of the pattern. This means that a uranium source of approximately 1.56x10^5 pCi/g would represent a pad concentration of approximately 171.6 pCi/g. While this level would produce good counting statistics, a concentration closer to the waste acceptance criteria (WAC) for the on-site disposal cell was preferable. It should also be noted that this source concentration represents the highest concentration that could be achieved while maintaining a close proximity to soil.

Since the goal was to produce a relatively flat flux and since the effect of not producing this is difficult to account for, the decision was made to use an area per source of 3292 cm^2. This produced an effective concentration of 326.5 pCi/g for uranium (approximately 979.5 ppm), which was near the WAC level, and a flatness factor of 0.985, which is nearly one.

APPENDIX C

PRODUCTION OF RADIOACTIVE STANDARDS
FOR THE RTIMP CALIBRATION PAD

1   **APPENDIX C**
2   **PRODUCTION OF RADIOACTIVE STANDARDS FOR THE RTIMP CALIBRATION PAD**
3

4   C.1 <u>INTRODUCTION</u>

5   This appendix describes the production of the radioactive sources used on the Real-Time Instrumentation

6   Measurement Program (RTIMP) calibration pad and to document their activity. The purchase of certified

7   standards from a commercial vendor was investigated, but the idea was abandoned because a vendor that

8   would provide certified sources containing the isotopes of interest could not be identified. A supplier of

9   certified uranium standards was identified, but the cost of purchasing the necessary quantities, assuming

10   they were available, would have been prohibitively high. The high estimated cost was due to both the

11   number of sources needed and the technical difficulties associated with certifying the desired isotopes.

12   As a consequence, Fluor Fernald personnel prepared the sources that were used to provide the gamma

13   flux for calibrating the various *in situ* gamma spectrometry systems.

14

15   This project was only possible because all three isotopes of concern (uranium-238, radium-226 and

16   thorium-232) were available at the FEMP. Various chemical forms of these materials have been stored at

17   the FEMP for many years. Well-established systems could be used to locate, sample and retrieve the

18   materials of interest. The quantity and purity of material available was also a prime consideration.

19

20   Producing calibration sources containing the isotopes of interest to the Soil Characterization and

21   Excavation Project has several advantages. Calibration measurements would then provide direct evidence

22   of each system's response to the isotopes of concern. Experimental information about the resolution of

23   each detector at each of the target isotope gamma energies would be gained. Having standards containing

24   the target isotopes also would make it possible to study interference effects among the various isotopes by

25   deploying multiple isotopes at the same time or combining single isotope spectra.

26

27   All of the factors listed above combined favorably to make the production of calibration pad standards at

28   the FEMP feasible.

29

30   C.2 <u>OVERVIEW OF THE SOURCE PRODUCTION PROCESS</u>

31   To minimize the possibility of leakage, solid matrix materials were chosen for the calibration pad sources.

32   Uranium tetrafluoride (UF_4, also known as green salt) was selected as the base ingredient for the uranium

33   standards because sufficient quantities of high purity material were available. The choices of materials

34   for the radium and thorium standards were more limited. K-65 Silo material was chosen to make the

1   radium-226 standard because surplus quantities of this material had already been retrieved from storage,

2   dried and homogenized for another project. Thorium dioxide was selected as the basis of the thorium-232

3   calibration pad standard because waste inventory records indicated that this was one of the few materials

4   in storage with the desired purity and quantity.

5

6   To produce sources suitable for use on the calibration pad, the pure standard material had to be diluted to

7   create material with the desired density and isotopic concentration. This ensured the gamma ray

8   attenuation properties of the standards would match those of the surrounding soil as closely as possible,

9   thereby arriving at a better simulation of uniform soil contamination. Each pure reference material was

10   analyzed in the Fluor Fernald Analytical Laboratory to determine its purity. The laboratory analysis

11   results were also used as a guide to compute a dilution ratio that would yield the desired density and

12   radionuclide concentration. In each case a diluent was used to lower the density and activity of the pure

13   reference material. Soil was used as a diluent for the radium and thorium sources, while dried ion

14   exchange resin proved to be more suitable for the uranium reference material.

15

16   Based on the gamma flux computations described in Appendix B of this report, it was decided to produce

17   50 standards and then select the best 45 standards for use on the calibration pad. Plastic core tubes with a

18   diameter of 1.25 inches and a height of 6 inches were chosen as the containers in which the reference

19   standards would be deployed on the calibration pad. The diluted source material that would be used to fill

20   each tube was mixed separately in the following manner. Fifty separate 250-mL plastic screw cap bottles

21   were filled with the desired amounts of pure standard material and diluent. The combined materials

22   filled approximately half the volume of the plastic bottles, leaving adequate room for the two dry solid

23   materials to mix together inside each bottle. The 250-mL plastic bottles were placed on a tumbler and

24   tumbled end-to-end for a minimum of three days. After tumbling the diluted mixture (standard material

25   plus diluent) from each bottle was transferred into a core tube, and the ends of the tubes were capped and

26   sealed with tape to prevent leakage. Each tube was weighed before and after it was filled so that the

27   amount of standard reference material added to each tube could be computed.

28

29   After the tubes were filled, each one was analyzed twice, except for five of the uranium tubes. Each tube

30   underwent spectral analysis by a shielded laboratory HPGe detector and also by one of the RTIMP *in situ*

31   HPGe detectors. The laboratory prepared a special jig to hold the tubes approximately two inches from

32   the end cap of the shielded HPGe detector. The lab also filled an extra core tube with a certified soil

33   reference material to produce a calibration standard in a configuration identical to that of the core tubes

34   containing the calibration pad sources. Every tenth sample was counted twice to provide duplicate

1 analyses. While counting the tubes with an *in situ* HPGe detector, the detector was not shielded and the

2 tubes containing the diluted source material were placed one meter away from the end cap of the detector.

3 With this arrangement, the cylindrical sources appeared to be point sources to the HPGe detector.

4

5 The uranium sources were processed first. After counting all 50 of the uranium sources with the *in situ*

6 detector, the mean uranium-238 concentration was computed, and the samples were ranked according to

7 the magnitude of the difference between the individual measured activity and the mean. The five

8 cylinders with the largest deviation from the mean were omitted from use on the calibration pad. The

9 remaining 45 uranium sources were then submitted for laboratory gamma spectrometry to obtain

10 independent uranium-238 measurements that would be defensible as "certified" values.

11

12 After processing the uranium standards, it was decided that it would be more appropriate to eliminate

13 sources from use on the calibration pad based on laboratory analyses rather than *in situ* detector results

14 because laboratory analyses which occur under more controlled conditions are generally more reliable.

15 Consequently the analysis sequence for the radium and thorium sources was reversed. All of the radium

16 and thorium sources were submitted for laboratory gamma spectrometry, and five sources were

17 eliminated from each set based on their deviation from the means of the laboratory analyses. Then the

18 remaining 45 sources in each set were analyzed as point sources with an *in situ* detector to corroborate the

19 laboratory results. For each set, the mean of the laboratory isotopic concentration of the 45 sources

20 actually deployed on the calibration pad was used as the known value in the gamma flux calculations.

21

22 C.3 <u>PREPARATION OF URANIUM SOURCES</u>

23 As noted in the previous section, uranium tetrafluoride, UF_4 (commonly known as "green salt"), was

24 chosen as the material from which to make the uranium standards. After retrieval of this material from

25 storage, two aliquots were analyzed for percent uranium by a volumetric technique and gamma emitting

26 radionuclides to verify the purity of the material. The laboratory results for the unadulterated material

27 retrieved from storage are given in the table below.

28

29 **PURE GREEN SALT ANALYSIS RESULTS**

30

Analysis	Sample 1	Sample 2
Percent Uranium	72.9%	72.8%
U-238 by Gamma Spectrometry	230000 pCi/g	220000 pCi/g

31

1   The gamma spectrometry also showed trace impurities of neptunium-237 and thorium-228 daughters, but

2   the levels of these contaminants were low enough that their presence would not create problems. Overall,

3   the results above indicate that the green salt was quite pure. The theoretical percentage of uranium in UF$_4$

4   is 75.8 percent.

5

6   The laboratory analysis results were used as a guide to compute a dilution ratio that would yield a

7   standard with the desired activity and density. Dilution of the uranium reference material presented more

8   of a challenge than the other two materials due to its higher density. Dried ion exchange resin was chosen

9   as the diluent because its low density (approximately 0.7 g/cm^3) would be very effective in reducing the

10   density of the final mixture to the desired range without having to add an inordinate amount of diluent.

11   A 2 to 1 mixture of green salt to dried resin (on a weight basis) was used to produce the diluted uranium

12   source material. This dilution yielded a material with attenuation properties similar to those of the

13   surrounding soil in the FEMP calibration pad. As stated above, the 45 uranium standards ultimately used

14   on the calibration pad were chosen on the basis of measurements with unshielded *in situ* HPGe detectors,

15   and laboratory measurements were used to derive the mean uranium concentration for these standards. In

16   both cases, the total uranium concentration was reported on the basis of the 1001 Kev gamma emission

17   from Pa-234m, which is the same gamma line that the RTIMP sodium iodide detectors use for

18   quantifying uranium.

19

20   Both the laboratory and the *in situ* gamma spectrometry results for the 45 uranium sources deployed on

21   the calibration pad are displayed in Table C-1 for comparison purposes. (Sources U19, U22, U25, U29

22   and U30 are missing from the table because these sources were not used on the calibration pad.) The total

23   uranium concentrations, listed in the "Laboratory Gamma Spec" column, were increased by 3 percent to

24   account for the difference in density (and therefore attenuation) between the laboratory soil calibration

25   standard and the diluted calibration pad standards. The *in situ* measurement results were generally higher

26   than the laboratory results, with the mean of the *in situ* results being 9 percent higher than the laboratory

27   mean. Although the *in situ* mean doesn't fall within the acceptable range defined by the laboratory mean

28   ±2 sigma, this is reasonable agreement considering the different conditions under which the

29   measurements were performed. The standard deviation of the laboratory measurements was considerably

30   smaller than that of the *in situ* measurements. The mean value of the Laboratory Gamma Spectrometry

31   results listed in Table C-1 was used as the known or "certified" value for the uranium standards in the

32   gamma ray flux computations. Table C-1 also lists the weight of diluted standard loaded into each tube

33   and the density of the material computed on the basis of a tube volume of 120.6 cm^3.

34

1   Impurity levels are an important consideration for a standard. The gamma spectra for all of the standards

2   were examined closely for evidence of impurity isotopes, particularly those that might cause interferences

3   when counting the standards with sodium iodide detectors. The spectra from all of the uranium standards

4   had two things in common. There were no spectral peaks from isotopes in the thorium-232 decay chain,

5   and there were no peaks from daughters of radium-226, even though they are members of the

6   uranium-238 decay chain. There were a number of photopeaks from protactinium-234, which is higher in

7   the uranium-238 decay chain than radium-226. The spectra from the uranium standards are characteristic

8   of a highly purified uranium compound, that is, a compound from which both thorium-232 and

9   radium-226 decay products have been removed. One would expect exactly these characteristics of green

10 salt, which was an intermediate product in the uranium metal production process carried out at Fernald.

11 In summary, protactinium-234 was the only prominent "contaminant" in the uranium standards. This

12 contaminant is unavoidable since protactinium-234 is the third daughter in the uranium-238 decay series,

13 and will be present to some degree in any aged uranium sample. There was no spectral evidence of

14 thorium-232 decay product contamination in the uranium standards

15

16 ## C.4 PREPARATION OF RADIUM SOURCES

17 K-65 Silo material which had previously been dried and homogenized by another project was selected for

18 use as a radium standard because of its high radium-226 activity. Two sample aliquots were submitted

19 for laboratory analysis to determine the purity of the material and to determine an appropriate dilution

20 factor. Because this material contained high levels of radium-226, two-gram aliquots were dissolved in

21 acid and diluted to 750 milliliters prior to performing gamma spectrometry analyses in the laboratory.

22 The laboratory results are shown below.

23

24 **UNDILUTED K-65 SILO MATERIAL ANALYSIS RESULTS**

25

Analysis	Sample 1	Sample 2
Ra-226 by Gamma Spectrometry	238000 pCi/g	249000 pCi/g

26

27 The results above were based on the 186.2 Kev photopeak emitted directly from radium-226, as opposed

28 to peaks from radium-226 daughters. Photopeaks from uranium-238, thorium-227 and radium-223 were

29 also identified in the gamma ray spectrum from each sample. However, the levels of these isotopes were

30 at least a factor of 35 lower than the radium-226 concentrations. After dilution, the presence of these

31 gamma-emitting isotopes would be unimportant.

32

1 Based on the laboratory results reported above, it was determined that a 1 to 25 dilution would be

2 appropriate for the radium source. In this case the chosen diluent was dried clay soil similar to that used

3 to construct the calibration pad. With a mixture ratio of one gram of K-65 Silo material to 25 grams of

4 soil, the density of the diluted radium standard would essentially be that of the clay soil, which was

5 measured to be 1.52 g/cm^3.

6

7 The 50 tubes containing the diluted radium standard were submitted for laboratory analysis by gamma

8 spectrometry. The samples were counted in the same containers (15 cm core tubes) that would be

9 deployed on the calibration pad using the special jig mentioned above to reproducibly position the

10 samples. Radium-226 has a number of gamma emissions that could be used to compute the radionuclide

11 concentration in each tube. There was generally good agreement among the activities calculated with the

12 various gamma lines. Since the sodium iodide *in situ* detectors use the 1764.5 Kev gamma line of

13 bismuth-214 to compute radium-226 activity, the value reported by the laboratory for this line was

14 adopted as the known value for the radium-226 standards. Because soil was used as a diluent in this case,

15 no compensation for density differences between the laboratory calibration standard and the samples was

16 necessary. The mean of the 50 laboratory radium-226 results was computed and the five sources with the

17 largest deviation from the mean were excluded from use. Sources RA1, RA16, RA29, RA30 and RA32

18 were excluded. Table C-2 contains the gamma spectrometry results for the remaining 45 radium-226

19 standards that were used for instrument calibrations on the calibration pad. Confirmatory *in situ* HPGe

20 results as well as laboratory results are displayed. Within experimental uncertainties, the two means are

21 not significantly different at the 95 percent confidence level. The mean of the *in situ* measurements was

22 99 percent of the laboratory mean, but the standard deviation of the lab results was significantly smaller

23 than the standard deviation of the *in situ* results. The average of the laboratory radium-226 concentrations

24 in the 45 tubes actually used on the calibration pad was used as the known or "certified" value for the

25 radium standards in the gamma ray flux computations. In addition to the dry weight radium-226 results,

26 the table also displays the weight and density of the radium bearing material in each standard.

27

28 The gamma spectra from the radium standards were examined closely for evidence of impurity isotopes.

29 The uranium-238 and thorium-227 that were identified in the undiluted samples were not evident in the

30 diluted standards. The only observable "contaminants" in the radium standards were radium-226

31 progeny, primarily lead-214 and bismuth-214, which are short-lived daughters of radon-222. These are

32 not true contaminants since the real time instruments use some of the bismuth-214 peaks to quantify

33 radium-226. There was no spectral evidence of uranium-238 daughters above radium-226 in the decay

1 series. Thorium-232 decay products were also absent from the radium standard spectra. In particular,

2 there were no prominent interferences that might cause problems when using sodium iodide detectors.

3

4 C.5 <u>PREPARATION OF THORIUM SOURCES</u>

5 After identifying thorium dioxide from waste management records as a candidate for thorium-232 source

6 material, an adequate supply was retrieved from storage. Two samples (a 1-gram and a 5-gram aliquot)

7 were submitted for laboratory analysis to determine the activity and the purity of the material. Because

8 this material contained high levels of thorium-232, each aliquot was dissolved in acid and diluted to

9 750 milliliters prior to performing gamma spectrometry analyses in the laboratory. The laboratory results

10 are shown below.

11

12 **UNDILUTED K-65 SILO MATERIAL ANALYSIS RESULTS**

13

Analysis	Sample 1	Sample 2
Th-232 by Gamma Spectrometry	52700 pCi/g	52400 pCi/g

14

15 The two sample aliquots contained uranium-238 at 3300 and 3800 pCi/g. Gamma ray peaks from

16 thorium-227 and radium-223, as well as thorium-232 and uranium-238 daughters, were also identified in

17 the two sample spectra. However, the levels of these impurity isotopes were not high enough to cause

18 problems, especially after the material was diluted.

19

20 Based on the laboratory results reported above, it was determined that a 1 to 10 dilution would be

21 appropriate for the thorium sources. Dry clay soil was used as a diluent for the thorium dioxide. With a

22 mixture ratio of 1 gram of thorium dioxide to 10 grams of soil, the density of the diluted standard would

23 essentially be that of the clay soil, which was measured to be 1.52 g/cm^3.

24

25 The 50 tubes containing the diluted thorium standard were submitted for laboratory analysis by gamma

26 spectrometry. The samples were counted in the 15-cm core tubes that would be deployed on the

27 calibration pad. Thorium-232 has a number of gamma emissions that can be used to compute the

28 radionuclide concentration, such as the 2614.5 Kev peak from thallium-208, a thorium-232 daughter. The

29 RTIMP sodium iodide detectors use this peak to calculate thorium-232 activity. The laboratory, however,

30 does not use this peak because their normal practice is to observe an energy range of 0 to 2000 Kev.

31 Within that energy range, a number of thorium-232 daughter peaks are available for calculation of

32 thorium-232 activity. The 911 Kev emission from actinium-228 was used as the basis for the

33 thorium-232 results reported by the laboratory. Once again, because soil was the diluent, no

1   compensation for density differences between the laboratory calibration standard and the samples was

2   necessary. The mean of the 50 laboratory thorium-232 results was computed and the five sources with

3   the largest deviation from the mean were excluded from use. Sources TH3, TH18, TH31, TH34 and

4   TH41 were excluded. The laboratory and the *in situ* gamma spectrometry results for the remaining

5   45 standards are shown in Table C-3. The *in situ* HPGe analyses were performed simply to confirm the

6   laboratory values. The mean of the *in situ* measurements was 86 percent of the laboratory mean, and the

7   standard deviation of the *in situ* measurements was about two times greater than the standard deviation of

8   the lab results. A student's t test shown that the *in situ* and lab mean values are statistically different. The

9   difference may be attributed, at least in part, to the fact that different gamma rays were used to compute

10   sample activity concentrations, although ideally the two photons should yield identical results. The

11   average of the laboratory thorium-232 concentrations in the 45 tubes actually used on the calibration pad,

12   5295 pCi/g, was used as the "certified" value for the thorium standards in the gamma ray flux

13   computations. The weight and density of each thorium standard is also shown in Table C-3.

14

15   The gamma spectra from the thorium standards were examined closely for evidence of impurity isotopes.

16   The spectra indicate that the thorium standard materials were highly purified. Only thorium-232 decay

17   products could be identified in the standard spectra, primarily actinium-228, lead-212, bismuth-212 and

18   thallium-208. These are not true contaminants since they are present in any aged thorium sample, and

19   their gamma lines are used by the real time instruments to quantify thorium-232. After mixing of the

20   thorium dioxide material with clay soil, the uranium-238, thallium-227 and radium-223 contamination

21   found in the pure material was no longer observable.

TABLE C-1
URANIUM SOURCES FOR RTIMP CALIBRATION PAD

Source Number	Standard Added (g)	Standard Density g/cm³	Lab Gamma Spec U-238 pCi/g	*In Situ* Gamma Spec (point source) U-238 pCi/g
U1	206.94	1.72	1.61E+05	1.92E+05
U2	214.48	1.78	1.56E+05	1.74E+05
U3	215.19	1.78	1.56E+05	1.74E+05
U4	207.58	1.72	1.60E+05	1.45E+05
U5	210.91	1.75	1.52E+05	1.66E+05
U6	211.07	1.75	1.57E+05	1.55E+05
U7	213.59	1.77	1.58E+05	1.66E+05
U8	211.15	1.75	1.57E+05	1.61E+05
U9	213.60	1.77	1.57E+05	1.53E+05
U10	209.79	1.74	1.59E+05	1.39E+05
U11	214.79	1.78	1.60E+05	1.41E+05
U12	212.99	1.77	1.55E+05	1.50E+05
U13	214.69	1.78	1.58E+05	1.60E+05
U14	205.99	1.71	1.61E+05	1.67E+05
U15	216.45	1.79	1.63E+05	1.47E+05
U16	216.32	1.79	1.57E+05	1.83E+05
U17	213.94	1.77	1.59E+05	1.72E+05
U18	209.07	1.73	1.55E+05	1.77E+05
U20	216.30	1.79	1.58E+05	1.54E+05
U21	216.63	1.80	1.57E+05	2.06E+05
U23	211.05	1.75	1.55E+05	1.84E+05
U24	211.06	1.75	1.51E+05	1.76E+05
U26	210.24	1.74	1.58E+05	1.59E+05
U27	206.31	1.71	1.58E+05	1.59E+05
U28	207.78	1.72	1.57E+05	1.93E+05
U31	216.43	1.79	1.59E+05	1.62E+05
U32	201.86	1.67	1.57E+05	1.80E+05
U33	218.13	1.81	1.59E+05	1.56E+05
U34	213.64	1.77	1.56E+05	1.39E+05
U35	215.27	1.78	1.58E+05	1.79E+05
U36	218.06	1.81	1.64E+05	1.61E+05
U37	195.11	1.62	1.41E+05	1.54E+05
U38	212.94	1.76	1.53E+05	1.57E+05
U39	207.28	1.72	1.64E+05	1.81E+05
U40	218.42	1.81	1.56E+05	1.81E+05
U41	211.62	1.75	1.57E+05	1.58E+05
U42	207.44	1.72	1.50E+05	1.77E+05
U43	211.06	1.75	1.59E+05	2.09E+05
U44	207.76	1.72	1.52E+05	2.08E+05
U45	214.53	1.78	1.52E+05	1.81E+05
U46	213.28	1.77	1.53E+05	1.98E+05
U47	206.41	1.71	1.51E+05	1.74E+05
U48	206.02	1.71	1.51E+05	1.76E+05
U49	213.20	1.77	1.56E+05	1.99E+05
U50	208.46	1.73	1.64E+05	1.59E+05
		Min	1.41E+05	1.39E+05
		Max	1.64E+05	2.09E+05
		Range	2.27E+04	7.00E+04
		Mean	1.56E+05	1.70E+05
		STD Dev	4.04E+03	1.82E+04
		%STD Dev	2.6%	10.7%

TABLE C-2
RADIUM SOURCES FOR RTIMP CALIIBRATION PAD

Source Number	Standard Added (g)	Standard Density g/cm³	Lab Gamma Spec Ra-226 pCi/g	In Situ Gamma Spec (point source) Ra-226 pCi/g
RA2	196.67	1.63	11460	11340
RA3	198.03	1.64	11330	10600
RA4	198.24	1.64	10920	10560
RA5	196.26	1.63	11150	9540
RA6	187.75	1.56	11190	9460
RA7	184.30	1.53	11550	9640
RA8	180.38	1.49	11250	10360
RA9	189.36	1.57	10880	9350
RA10	187.37	1.55	11030	10070
RA11	193.73	1.61	11100	12390
RA12	186.73	1.55	10840	11060
RA13	180.39	1.50	10740	10190
RA14	184.40	1.53	11190	11770
RA15	186.05	1.54	10570	11070
RA17	207.89	1.72	11050	11010
RA18	211.63	1.75	11050	11880
RA19	204.05	1.69	11030	11720
RA20	208.04	1.72	10950	10980
RA21	206.25	1.71	10710	10510
RA22	193.66	1.61	11180	10020
RA23	202.21	1.68	10960	12400
RA24	190.65	1.58	11450	12600
RA25	192.19	1.59	11170	11900
RA26	185.22	1.54	11250	12940
RA27	187.10	1.55	11900	10890
RA28	182.13	1.51	11770	11150
RA31	207.00	1.72	11190	11430
RA33	206.40	1.71	10970	10920
RA34	200.82	1.66	11380	12370
RA35	200.70	1.66	11270	11790
RA36	198.48	1.64	11480	11910
RA37	199.85	1.66	11050	11870
RA38	200.61	1.66	11170	10670
RA39	199.31	1.65	11470	10720
RA40	201.60	1.67	11500	11710
RA41	200.12	1.66	11190	9934
RA42	200.32	1.66	11330	10380
RA43	202.14	1.68	11330	12050
RA44	202.90	1.68	11090	13070
RA45	195.98	1.62	11490	10670
RA46	196.13	1.63	11460	10710
RA47	192.95	1.60	11810	10850
RA48	197.92	1.64	11140	10530
RA49	192.36	1.59	11360	11560
RA50	188.63	1.56	11040	10520
		Min	10570	9350
		Max	11900	13070
		Range	1330	3720
		Mean	11209	11090
		STD Dev	280	930
		%STD Dev	2.5%	8.4%

TABLE C-3
THORIUM SOURCES FOR RTIMP CALIIBRATION PAD

Source Number	Standard Added (g)	Standard Density g/cm³	Lab Gamma Spec Th-232 pCi/g	In Situ Gamma Spec (point source) Th-232 pCi/g
TH-1	184.57	1.53	5050	3604
TH-2	186.10	1.54	5290	4526
TH-4	188.09	1.56	5310	4540
TH-5	185.40	1.54	5170	4480
TH-6	183.28	1.52	5000	4214
TH-7	184.72	1.53	5190	3676
TH-8	189.16	1.57	5320	4508
TH-9	188.73	1.56	5040	4768
TH-10	192.72	1.60	5250	4365
TH-11	197.81	1.64	5240	4603
TH-12	195.27	1.62	5020	4081
TH-13	199.34	1.65	4980	4810
TH-14	198.33	1.64	5140	4249
TH-15	192.29	1.59	5070	4144
TH-16	193.42	1.60	5010	4295
TH-17	196.20	1.63	5100	4475
TH-19	194.15	1.61	5200	4525
TH-20	192.22	1.59	5160	5228
TH-21	189.14	1.57	5560	4516
TH-22	196.07	1.62	4980	4476
TH-23	200.48	1.66	5160	4147
TH-24	197.87	1.64	5390	4613
TH-25	196.69	1.63	5580	5295
TH-26	194.76	1.61	5390	5105
TH-27	194.54	1.61	5350	4390
TH-28	196.44	1.63	5230	4826
TH-29	196.12	1.63	5390	4775
TH-30	196.33	1.63	5580	5001
TH-32	190.15	1.58	5450	5039
TH-33	193.20	1.60	5500	5318
TH-35	190.61	1.58	5430	4605
TH-36	191.56	1.59	5010	4456
TH-37	194.25	1.61	5610	5418
TH-38	201.07	1.67	5340	4286
TH-39	198.30	1.64	5630	4462
TH-40	205.09	1.70	5220	4421
TH-42	196.22	1.63	5550	4564
TH-43	192.56	1.60	5370	4651
TH-44	198.43	1.64	5350	4285
TH-45	197.04	1.63	5500	4491
TH-46	206.06	1.71	5360	4457
TH-47	200.59	1.66	5320	4463
TH-48	199.59	1.65	5470	5041
TH-49	198.08	1.64	5430	4402
TH-50	198.59	1.65	5570	4860
		Min	4980	3604
		Max	5630	5418
		Range	650	1814
		Mean	5295	4566
		STD Dev	194	383
		%STD Dev	3.7%	8.4%

APPENDIX D

POINT SOURCE CALIBRATION

1   **APPENDIX D**
2   **POINT SOURCE CALIBRATION**
3

4   D.1 <u>THEORY</u>

5   The NaI point source calibration is based on the HPGe point source calibration. Due to the shape of the

6   detector, the theory must be modified slightly. The HPGe detectors are cylindrical in shape and they are

7   utilized with the end of the cylinder facing down towards the soil. In this configuration, the electronics

8   and the liquid nitrogen dewer are above the detector so they do not interfere with the gamma flux coming

9   from the source. The NaI detectors are rectangular in shape with dimensions of 4-inch by 4-inch by

10   16-inch. The detector is oriented so that a 16-inch by 4-inch side is facing the soil making the detector

11   4 inches high. The NaI detector also has a photomultiplier tube mounted on one of the 4-inch by 4-inch

12   sides, which puts it within the path taken by some of the gamma flux arriving from the soil. The theory

13   behind the HPGe calibration assumes the detector is symmetrical; however, this assumption is clearly

14   inaccurate for the NaI detectors.

15

16   In order to modify the HPGe calibration theory to account for the asymmetrical nature of the NaI

17   detectors, it is necessary to derive the HPGe theory from the start.

18

19
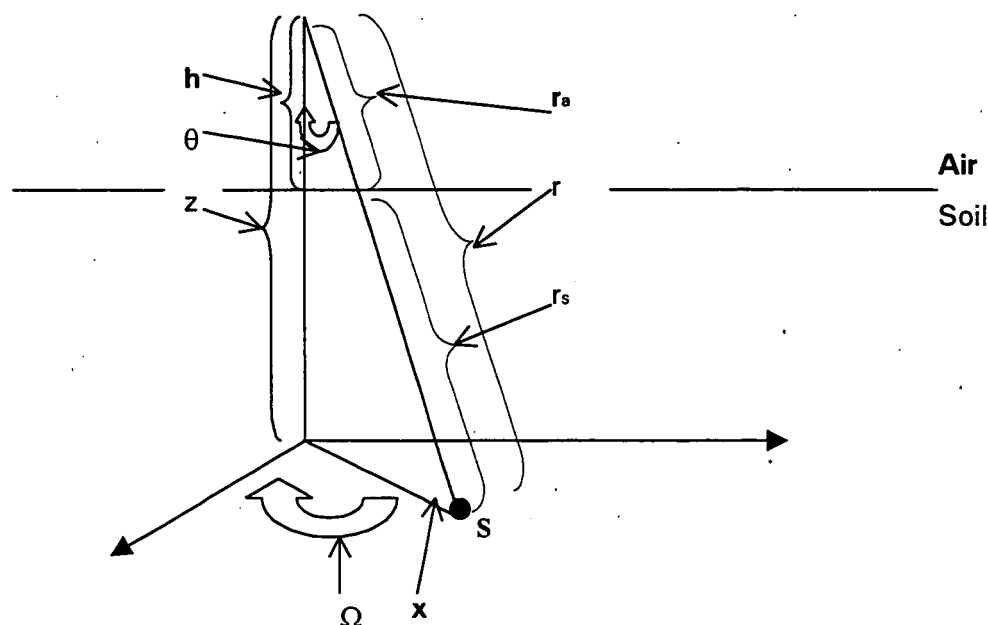
1   The drawing above is used to describe the gamma flux arriving at a point from an infinitely large

2   half-space with homogeneous concentration of activity. From the drawing, a mathematical equation can

3   be derived for this flux from the differential source at point S. This equation can then be integrated over

4   the entire volume of the half-space to determine the flux.

5

6   If any attenuation due to air or soil is ignored, the flux arriving at the detector from the differential

7   volume can be described as:

8

9    $Sv/(4*\pi*r^2)$

10

11   where:

12

13   Sv = The gammas per sec per cc emitted by the source

14   r = the distance between the source and the detection point.

15

16   Letting r_a and r_s represent the distance the gamma will travel in air and soil respectively, the attenuation

17   can be accounted for by using the following terms:

18

19    $e^{-(\mu/\rho)a*\rho a*ra} * e^{-(\mu/\rho)s*\rho s*rs}$

20

21   where:

22

23   μ/ρ = the mass attenuation coefficient, the subscripts representing air and soil.

24   ρ = the density, the coefficients representing air and soil

25   r = the distance the gamma will travel in each material.

26
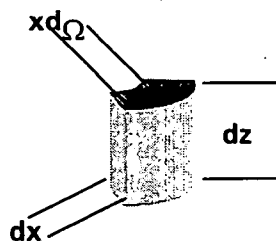
27   The drawing above shows the detail of the differential volume. From this, the differential volume can be

28   described as $x*d\Omega*dx*dz$. Putting this all together and integrating over the volume gives:

29

1

$$\phi = 2 \cdot \int_0^\pi \int_0^\infty \int_h^\infty \frac{Sv}{4 \cdot \pi \cdot r^2} \cdot e^{-\left(\frac{\mu a}{\rho a}\right) \cdot \rho a \cdot ra} \cdot e^{-\left(\frac{\mu s}{\rho s}\right) \cdot \rho s \cdot rs} \cdot x \, d\Omega \, dx \, d$$

2   Equation D-1

3

4 Where Ω is integrated from zero to π and the results multiplied by 2. Now putting all the variables in

5 terms of z, Ω, and θ, and allowing $\omega = 1/\cos\theta$ and allowing h to represent the detector height, the equation

6 becomes:

7

8

$$\phi = \frac{Sv}{2 \cdot \pi} \cdot \int_0^\pi \int_1^\infty \int_h^\infty \frac{1}{\omega} \cdot e^{-\left(\frac{\mu a}{\rho a}\right) \cdot \rho a \cdot h \cdot \omega} \cdot e^{-\left(\frac{\mu s}{\rho s}\right) \cdot \rho s \cdot (z - h) \cdot \omega} \, d\Omega \, d\omega \, d$$

9   Equation D-2

10

11 Integrating the above equation over z leads to the following equation.

12

13

$$\phi = \frac{Sv}{2 \cdot \pi \cdot \left(\frac{\mu s}{\rho s}\right) \cdot \rho s} \cdot \int_0^\pi \int_1^\infty \frac{e^{-\left(\frac{\mu a}{\rho a}\right) \cdot \rho a \cdot h \cdot \omega}}{\omega^2} \, d\Omega \, d\omega$$

14   Equation D-3

15

16 At this point, this equation can be integrated over Ω and ω to obtain the familiar equation for the flux

17 from an infinitely large homogeneous half-space:

18
19

20

$$\phi = \frac{Sv \cdot \left(\frac{\mu a}{\rho a}\right) \cdot \rho a \cdot h}{\rho s \cdot 2 \cdot \left(\frac{\mu s}{\rho s}\right)} \cdot \left[\frac{e^{-\frac{\mu a}{\rho a} \cdot \rho a \cdot h}}{\left(\frac{\mu a}{\rho a}\right) \cdot \rho a \cdot h} - E1\left[\left(\frac{\mu a}{\rho a}\right) \cdot \rho a \cdot h \right] \right]$$

21   Equation D-4

22
23

24 D.2 <u>CALIBRATION</u>

25 The factors affecting the detector response to a source of radioactivity can be described as follows:

26

27 $N_f/A = N_o/\phi * N_f/N_o * \phi/A$

28   Equation D-5

29

1   where:

2

3   N_f/A is the detector net count rate per activity concentration in the soil (cps/[pCi/gm] or cps/[ppm]). This

4   is the conversion factor being sought out during the calibration. It is essentially the detector efficiency

5   since the corrected net count rate would be divided by this in order to obtain the activity concentration.

6

7   ϕ/A is the flux expected at the detector from a particular source geometry divided by the activity

8   concentration of that source (gammas/[sec*cm^2]/[pCi/gm]). In this case, that is the calculated flux per

9   pCi/gm at the detector from a homogeneous infinite half-space. This term is not detector specific and is,

10 in fact, the homogeneous equation (Equation 4) divided by the source concentration (Sv/ρ_s) and the

11 appropriate gamma yield and .037, the conversion factor from disintegration's per second to pCi.

12

13 N_o/ϕ is the detector response to the flux from a known source normal to the detector face. That is the net

14 count rate obtained from a point source centered under the detector at a particular distance. In order to

15 obtain this value, the flux is determined by first determining the activity of the source being used in

16 disintegrations per second. This is requires decay correcting it if necessary. The activity is then

17 multiplied by the yield of the particular gamma ray of interest and then divided by $4*\pi*r^2$ to account for

18 the isotropic emission of the gamma rays. Lastly, this is multiplied by a term to account for the

19 attenuation of the gamma in air. The net count rate N_o, is simply the net counts (Net) divided by the live

20 time (LT). The equation for this term appears below.

21

22 $N_o/\phi = Net*4*\pi*r^2/(LT*Act*\gamma)*e^{([\mu/\rho]*\rho*r)}$

23   Equation D-6

24

25 where:

26

27 Net =   Net counts for the peak (counts)

28 r   =   The distance between the detector and the source (cm)

29 LT =   Live time (sec)

30 Act =   Decay corrected source activity (dps)

31 γ =   the yield of the gamma ray of interest (γ / disintegration)

32 μ/ρ =   The mass attenuation coefficient of air for the gamma ray energy of interest (cm^2/gm)

33 ρ =   The density of air (gm/cc)

34

35 N_f/N_o is the net count rate averaged over all the angles of interest from a particular source at a particular

36 distance from the detector divided by the net count rate normal to the detector. This average net count

37 rate is weighted for importance of each angle. This term represents a ratio of the net count rate expected

38 from the infinite half-space to the net count rate obtained from a point source normal to the detector face.

1   In this way $N_o/\phi * N_f/N_o$ is the detector response if the flux from the source was coming from all angles of

2   interest in the same ratio as would be seen from a infinite half-space geometry. The equation for

3   determining N_f/N_o is:

4

5

$$\frac{Nf}{No} = \frac{2}{\phi} \cdot \int_0^\pi \int_0^{\frac{\pi}{2}} \phi(\theta,\Omega) \cdot \frac{N(\theta,\Omega)}{No} \, d\Omega \, d\theta$$

6   Equation D-7

7

8   Where again, Ω is determined from 0 to π and the result multiplied by two. $N_{(\theta,\Omega)}/N_o$ is the ratio of net

9   count rate at a particular angle to the net count rate at the reference position ($\theta = 0$). The particular angle

10   is a function of two angles.

11

12   In order to determine this term, the above equation is modified to allow numerical integration. Since we

13   are ready know the equation for $\phi(\omega,\Omega)$, it is convenient to modify the above equation to put it in terms of

14   ω instead of θ. This can be done by simply expressing $N(\theta,\Omega)$ as $N(\omega,\Omega)$ and changing the limits of

15   integration to get:

16

17

$$\frac{Nf}{No} = \frac{2}{\phi} \cdot \int_0^\pi \int_1^\infty \phi(\omega,\Omega) \cdot \frac{N(\omega,\Omega)}{No} \, d\Omega \, d\omega$$

18   Equation D-8

19

20   The equation for $\phi(\omega,\Omega)$ is simply equation 3 without any integration so the numerical form of equation 8

21   above is:

22

23

$$\frac{Nf}{No} = \frac{2 \cdot Sv}{\phi \cdot 2 \cdot \pi \cdot \left(\frac{\mu s}{\rho s}\right) \cdot \rho s} \cdot \sum_{\Omega=0}^{\pi} \sum_{\omega=1}^{\infty} \frac{N(\omega,\Omega)}{No} \cdot \frac{e^{-\left(\frac{\mu a}{\rho a}\right) \cdot \rho a \cdot h \cdot \omega}}{\omega^2} \cdot \Delta\Omega \cdot \Delta\omega$$

24   Equation D-9

25

26   Since we already know the equation for ϕ (equation 4), we can insert that into the above equation and

27   cancel out several terms:

28

1

$$\frac{Nf}{No} = \frac{2 \cdot \sum\limits_{\Omega=0}^{\pi} \sum\limits_{\omega=1}^{\infty} \frac{N(\omega,\Omega)}{No} \cdot \frac{e^{-\left(\frac{\mu a}{\rho a}\right) \cdot \rho a \cdot h \cdot \omega}}{\omega^2} \cdot \Delta\Omega \cdot \Delta\omega}{\pi \cdot \left(\frac{\mu a}{\rho a}\right) \cdot \rho a \cdot h \cdot \left[\frac{e^{-\left(\frac{\mu a}{\rho a}\right) \cdot \rho a \cdot h}}{\left(\frac{\mu a}{\rho a}\right) \cdot \rho a \cdot h} - E1\left[\left(\frac{\mu a}{\rho a}\right) \cdot \rho a \cdot h\right] \right]}$$

2

Equation D-10

3

4 Since a number of terms are not angle dependant, it is convenient at this point to multiply the Nf/No term

5 with the ϕ/A term to obtain the following equation:

6

7

$$\frac{Nf}{No} \cdot \frac{\phi}{A} = \frac{1}{\left[\pi \cdot \left(\frac{\mu s}{\rho s}\right)\right]} \cdot \sum\limits_{\Omega=0}^{\pi} \sum\limits_{\omega=1}^{\infty} \frac{N(\omega,\Omega)}{No} \cdot \frac{e^{-\left(\frac{\mu a}{\rho a}\right) \cdot \rho a \cdot h \cdot \omega}}{\omega^2} \cdot \Delta\Omega \cdot \Delta\omega$$

8

Equation D-11

9

10 $N(\omega,\Omega)/No$ is determined by measuring a source at various angles and dividing the net count rate by the

11 net count rate obtained at the reference position ($\theta = 0$). Since we are using numerical integration, the

12 smaller the increments used to determine Nf/No, the less error there will be in the calculation but also the

13 more values of $N(\omega,\Omega)$ that must be determined. As a compromise between accuracy and reality, the

14 equation can be divided up into 1-degree increments but the value of Nf/No measured with a source for

15 only a few of these angles. The rest of the values for Nf/No can be interpolated from the data that is

16 measured. This requires enough values of Nf/No be measured to allow for the construction of a smooth

17 curve.

18

19 In order to determine the necessary number of measurements to obtain a smooth curve, the data from

20 RTIMP test #3 (symmetry test) was used. This test only used cesium-137 and only tested the angles

21 around the detector centerline ($\theta=90$ degrees) and the angles around the detector with the source on the

22 ground ($\theta = 75.5$ degrees). With only two angles of θ measured, the smoothness of the curve with respect

23 to θ can not be determined directly. However, due to the dimensions of the detector, the measured angles

24 should be the worst case for angular dependence. After plotting a chart of the net counts per second

25 versus the angle, it was clear that 30-degree increments should be sufficient to approximate a smooth

26 curve. The two charts below depict the actual measurements compared to the 30-degree increment

27 interpolation measurements for both angles of θ.

1   **DETECTOR ANGULAR RESPONSE AT GROUND LEVEL**

2
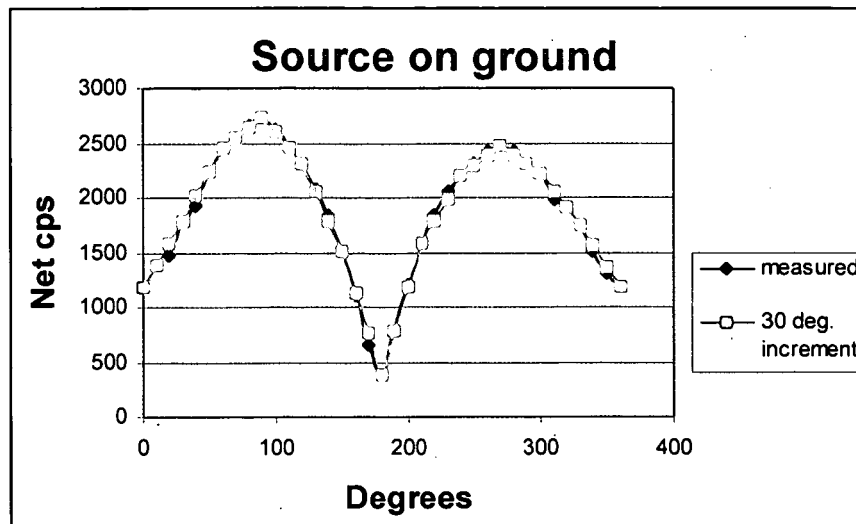
3   **DETECTOR ANGULAR RESPONSE AT DETECTOR CENTERLINE**

4
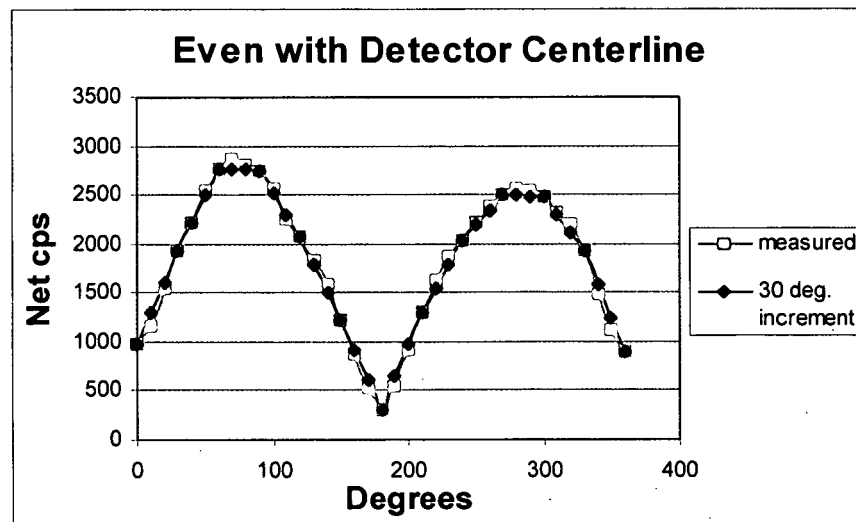
5   From the charts, it is clear that the difference between measuring a source every 10 degrees and

6   measuring it every 30 degrees is small. The charts however, indicate the peak count rate at 90 degrees is

7   higher than the count rate at 270 degrees while these two measurements would be expected to be nearly

8   equivalent. As pointed out in the test report, this is a possible indication of the detector not being

9   centered in the housing. Whatever the reason, it is important that the exact location of the detector be

10   known during the measurement. With the exact location known, it is believed that the two distinct arcs of

11   these charts will match much more closely and eliminate any need for measuring all 360 degrees around

12   the detector during calibration. It is, however, clear that 180 degrees of measurement are necessary since

13   there is a significant difference between the 0, 90, and 180-degree points. This all indicates that we

1 should be able to measure sources in 30-degree increments in the range of 0 to 180 degrees for Ω and 0 to

2 90 degrees for θ. The 0 and 180 degree measurements for Ω must be at the 4-inch by 4-inch ends of the

3 detector. This gives a total of 22 measurement locations required for the calibration. In any case, the

4 "smoothness" of the curves will have to be evaluated after the data is collected to ensure the number of

5 measurements was adequate to create a smooth curve.

6

7 ## D.3 FULL ABSORPTION PEAK VERSUS NET COUNTS

8 The ROIs for the NaI system are set at particular channels. The channels that were chosen were based on

9 two criteria. One, the most obvious, is to include all or most of the photopeak within the ROI. The

10 second was to adjust the ROI to eliminate as much interference as possible from other isotopes. Because

11 two criteria were used, the ROI does not necessarily include the entire photopeak. Since the efficiency

12 calibration does include the entire photopeak, this affect requires an adjustment to be made to the

13 efficiency.

14

15 The adjustment factor is easily determined with a point source of the isotope of concern. In our case that

16 is uranium-238, radium-226, and thorium-232. In order to determine this factor, the point source is

17 counted at the reference geometry. The net counts for the isotope is then determined normally but the full

18 absorption peak is also determined. A ratio of these two values then gives the fraction of the full

19 absorption peak that is accounted for in the net counts.

20

21 The efficiency (N_f/A) is then multiplied by this factor in order to correct for this effect. The N_f was

22 described earlier as the net counts expected from an infinitely large homogeneous source of activity "A".

23 In reality, it is the full absorption peak rather than the net counts. This is true because in determining this

24 factor, every peak measured was the full absorption peak. The correction we are actually looking for is

25 for the net counts determined in the field rather than the full absorption peak. By multiplying the

26 efficiency by the adjustment factor, the net counts expected from the source would be lowered by the

27 fraction of the isotope peak actually being accounted for. In this way, the net count versus full absorption

28 peak affect is corrected.

29

30 ## D.4 POINT DETECTOR VESUS REAL DETECTOR

31 The theory above is based on a detection point while in reality the detector has volume. It must be

32 determined from where on the detector the distance and angle will be measured.

1   To examine the extent to which a measurement scheme represent a point detector, a first step must be to

2   determine a measurement scheme to analysis. The one analyzed here is to use the point at the center of

3   the bottom of the detector from which to measure the distance and the angles. With that in mind, the

4   distance to various points on the detector can be calculated. The worst case to consider is depicted in the

5   drawing below. It shows the longest dimension of the detector since that will affect the distance between

6   the source and the detector the most.

7
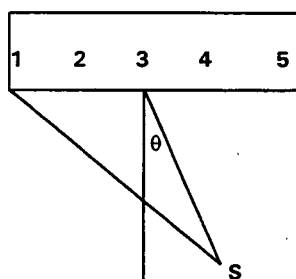
8   This drawing shows a source at point S and at angle θ from the center point of the bottom of the detector.

9   The one additional line represents the distance from the source to point #1. Point #3 is the center of the

10   detector and it is the point form which the distance and angles are measured. The distance to each point

11   on the detector as well as the average of all five points is shown on the chart below for each angle θ from

12   0 to 90 degrees.

13

14   **DISTANCE TO VARIOUS POINT ON DETECTOR WITH NOMANAL DISTANCE OF 100CM**

Angle	R1	R2	R3	R4	R5	Average
0	101.9804	100.4988	100	100.4988	101.9804	100.9917
10	105.3309	102.212	100	98.75578	98.51603	100.9629
20	108.4808	103.8462	100	97.03587	95.03641	100.8799
30	111.3553	105.3565	100	95.39392	91.65151	100.7515
40	113.891	106.7032	100	93.88517	88.48079	100.592
50	116.0352	107.8522	100	92.56301	85.64941	100.42
60	117.7459	108.7752	100	91.4765	83.28204	100.2559
70	118.9906	109.4504	100	90.66761	81.49374	100.1205
80	119.7465	109.8618	100	90.16864	80.37891	100.0312
90	120	110	100	90	80	100

15

1 The values in the chart above are in centimeters with the distance from the source to the center point of

2 the detector being 100 cm. An additional chart below indicates the values if the distance where to be

3 31 centimeters.

4

5 **DISTANCE TO VARIOUS POINT ON DETECTOR WITH NOMANAL DISTANCE OF 31CM**

Angle	R1	R2	R3	R4	R5	Average
0	36.89173	32.57299	31	32.57299	36.89173	33.98589
10	39.70294	34.1857	31	30.87617	33.84784	33.92253
20	42.2505	35.67986	31	29.1367	30.60874	33.73516
30	44.50843	37.02702	31	27.40438	27.22132	33.43223
40	46.45489	38.20377	31	25.73853	23.74749	33.02894
50	48.07177	39.19117	31	24.20852	20.27572	32.54944
60	49.34442	39.97419	31	22.89245	16.94487	32.03118
70	50.2615	40.54145	31	21.87214	13.99218	31.53346
80	50.81497	40.88497	31	21.22308	11.82533	31.14967
90	51	41	31	21	11	31

6

7 It can be seen from the charts that in the case of the 31 cm distance, the average distances to all points on

8 the detector differs from 31 cm by almost 10 percent (33.99 cm) while the 100 cm case differs by less

9 than 1 percent. Generally, the source will behave as a point source if the distance between it and the

10 detector is at least three times the longest dimension of the source. It would appear that the same rule

11 would work for detectors also to indicate when it will behave as a point detector. Since the longest

12 dimension of the detector is 40 cm, this rule indicates a distance of 120 cm is suitable. However, since it

13 is only a rule of thumb, and the analysis above indicates 100 cm is acceptable, a distance of 100 cm was

14 used for the purpose of calibrating the NaI detectors. The sides of the detector were not considered

15 during this evaluation. This was done because the importance of the sides is unclear in this evaluation

16 leading to a fear that the including sides would skew the results. It is important to keep in mind that for

17 most of the counts, the entire bottom and two of the sides will be directly "visible" to the source. It

18 should also be noted that any error introduced by having the source closer to the ends of the detector are

19 minimized by the fact that, when these ends have the most affect on the net counts, they are at such an

20 angle that the flux from that angle is least important. In addition, the Nf/No effectively provides a

21 geometry correction that accounts for the detector response to various angles. This term should inherently

22 provide a correction for the non-point nature of the detector.

23

1   D.5 <u>INTERFERENCE FACTOR DETERMINATION</u>

2   The corrected net count rate is divided by the efficiency (N_f/A) to obtain the activity concentration in the

3   soil. The corrected net count rate is the corrected net counts divided by the live time. The corrected net

4   counts are the net counts corrected for the influence of interfering isotopes. This correction was discussed

·5   in detail in Appedix A where the basic equations were listed as:

6

7   $U_{cnet} = U_{net} - k1*Ra_{cnet} - k2*Th_{cnet}$
8   $Ra_{cnet} = Ra_{net} - k3*U_{cnet} - k4*Th_{cnet}$
9   $Th_{cnet} = Th_{net} - k5*U_{cnet} - k6*Ra_{cnet}$

10   Equation D-12

11

12   Where the "cnet" subscript represents corrected net counts and the "net" subscript represents raw net

13   counts. The "k" factors are the interference coefficients. The k-factor is a ratio of the net counts that

14   accumulate in two different regions from one isotope assuming the isotope is in the same geometry being

15   calibrated for. In our case, that means an infinitely large homogeneous geometry. Since during a point

16   source calibration this geometry does not exist, some additional steps must be taken to determine these

17   factors.

18

19   We can take advantage of the calibration effort already discussed in this document to determine these

20   interference coefficients by noting that the N_f in the N_f/ N_o term is the net counts expected from an infinite

21   source. This implies the k-factor would simply be a ratio of these two values. $K = N_{f1}/ N_{f2}$. Since $N_{f1} =$

22   $N_{f1}/ N_{o1} * N_{o1}$, a working equation for the k-factor can be determined to be:

23

24   $K = N_{f1}/ N_{f2} = [N_{f1}/ N_{o1}] / [N_{f2}/ N_{o2}] * N_{o1}/ N_{o2}$

25   Equation D-13

26

27   The second term (N_{o1}/ N_{o2}) is simple the ratio of net interference counts to the net counts in the isotope

28   ROI from a point source at the reference point. N_f/ N_o has already been determined for several energies

29   as part of the calibration process. A curve can be drawn of this factor versus energy to interpolate the

30   value necessary in determining the k-factors. The choice at this point is to decide what energy to use

31   since more than one gamma ray contributes to the interference. It would be very difficult to attempt to

32   determine the affect of each gamma since there is only one measured quantity of the portion of each peak

33   that falls within the ROI. Without knowing how much each individual peak contributes, it is not possible

34   to use more than one energy in the k-factor calculation. This proportion could theoretically be estimated

35   however, N_f/ N_o is expected to be relatively flat at the energies of interest to us (>about 1001 kev). This

1   means that regardless of what energy is chosen, as long as it is within or close to the ROI energy, the error

2   associated with this choice should be small. This implies the centroid energy for the ROI of interest could

3   be used with little error. Since this is the location of the ROI, it would make since that this would be a

4   good average of the energies that contribute interference to that ROI. A more correct method, however,

5   would be to evaluate each situation of interfering isotopes and determine the most appropriate energy.

6   This is done later in this section.

7

8   It should be noted at this point that N_{o1}/N_{o2} is determined using net counts in the particular regions of

9   interest while the Nf/No terms are determined using the full absorption peak. Effectively, Nf/No is the

10   ratio of the counts from an infinite homogeneous source divided by the counts from a point source. Since

11   the ROI only measures a fraction of the full absorption peak, these counts should be reduced by this

12   fraction. Since both the top and the bottom portions of the ratio would have to be reduced by the same

13   fraction, it can be said that Nf/No is the same for both the full absorption peak and one determined using

14   the ROIs. Since the No1/No2 term is already determined using the ROIs, the K-factor determined in

15   Equation 13 is actually the ratio of the net counts from the ROIs not the full absorption peak. This is in

16   fact the term we are really interested in for the K-factor since the net counts using the ROIs are what will

17   be determined in the field and what will need to be corrected for interference.

18

19   Several factors influence the interference coefficients. Overall, the k-factor is a simple ratio of the net

20   counts in two different regions. This ratio will, however, vary with the amount of shielding placed

21   between the detector and the source. This is true because the two ROI can represent significantly

22   different energies, 1001 kev versus 2614 kev for example. Since most of these factors are accounted for

23   in the efficiency determination, the above equation will account for most of these factors. In this way,

24   any angular dependence on detector efficiency, attenuation, etc. can be ignored. The only item that is not

25   accounted for is the affect of angular dependence on detector resolution. This is true since in order to

26   determine the values of N_f/N_o, the entire peak must be accounted for. This implies that any resolution

27   affect that might widen the peak would be ignored. In the case of k-factors, only portions of many of the

28   interference peaks are measured in the ROI. This implies that if the resolution varies with incident angle,

29   the above equation would not account for it.

30

31   The resolution of each spectra used in RTIMP test #3 (the symmetry test) was determined. This test

32   counted a cesium-137 source 1.2 meters from the RSS detector. The source was placed on the ground and

33   moved in 10-degree increments in a full circle around the detector. These counts were then repeated with

34   the source elevated above the ground 36 cm so that it was level with the detector centerline. The

1   resolution from these counts was determined (in number of channels) and plotted against the angle.

2   These plots are shown below in Figure 3 and 4.

3

4   **RESOLUTION VS ANGLE AT GROUND LEVEL**

Source place on ground

5
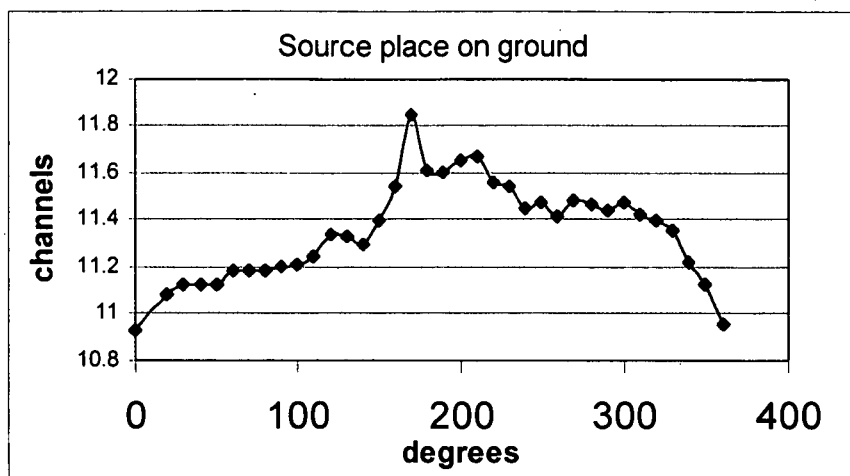
6   **RESOLUTION VS ANGLE AT DETECTOR CENTERLINE**

source even with detector centerline

·7

8
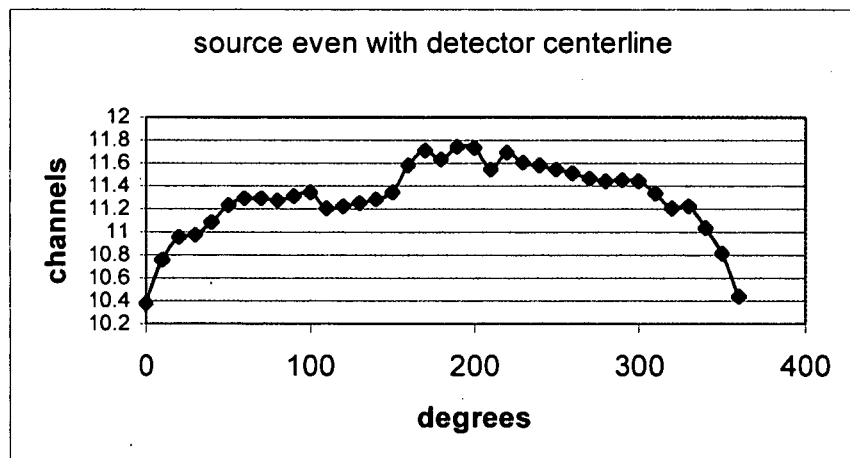
9   The graph shows that there is some angular dependence for the resolution. However, it should be noted

10 that the most significant variations occur near the ends of the detector (0, 180 and 360 degrees). In

11 comparing the two charts, it can be seen that this affect is more significant when the source is even with

12 the detector centerline. This implies that the charts above depict the worst case and that the variations in

13 resolution for different angles of θ will be less. The ends of the detector also happen to be the location

14 with the fewest net counts which implies their importance is small.

15

1 If a point source is measured at the reference point, it should be equivalent to the 90-degree measurement

2 on Figure 4 above. This value is 11.31 channels. The average of all the measurements from both plots is

3 11.32 channels. This implies one measurement taken at the reference point would represent a good

4 average resolution. The difference between the individually measured resolutions and the reference value

5 (11.31) is <5 percent for all but four measurements. These measurements are the four lowest

6 measurement on the ends of Figure 2 and as already mentioned, have the lowest importance. Also, over

7 83 percent of the measurements varied from the reference value by less than 3 percent. All of this

8 together implies that the angular dependence of the resolution is small enough to safely ignore.

9

10 The appropriate energy to use when determining the value of N_{f1}/N_{f2} for the interfering gammas is best

11 sorted out case by case. The individual k values from Equation 12 are discussed below.

12

13 The coefficient k1 is the radium interference on the Uranium ROI. The largest affect of these gammas is

14 from the 1120 kev and 934 kev gammas. The 1120 kev gamma has a higher yield but a smaller portion of

15 it is actually in the uranium ROI. The midpoint between these gammas is 1027 kev. Considering how

16 close this is to the 1001 kev centroid of the uranium ROI and the fact that there are a number of other

17 lower yield gammas surrounding this ROI, the 1001 kev energy should be a good representative energy

18 and should be used to determine this k factor.

19

20 The coefficient k2 is the thorium interference on the uranium ROI. By far the most influential gammas in

21 this situation are the 911 and the 969 kev peaks however, the combined peak for all these gammas has a

22 centroid of approximately 923 kev. Therefore, this is the energy that should be used in determining the k

23 value.

24

25 The coefficient k3 is the Uranium interference on the Radium ROI. There are no uranium gammas of

26 significant yield in the radium regions. However, there are a number of low yield gammas in each region.

27 There are at least nine that affect the lower background region while the upper background region is

28 affected by at least five and the ROI itself is affected by 14. Some of these gammas affect more than one

29 of the regions listed. Since they appear to be evenly distributed with energy and yield the 1765 kev

30 centroid should be used as the energy for calculating this k-factor.

31

32 The coefficient k4 is the thorium interference on the Radium ROI. While none of the gammas have a very

33 large yield, the 1620 and 1630 kev gammas have by far a larger yield than the others. These two gammas

34 however, fall below even the lower background region so only a portion of these peaks affect the net

1 thorium counts. Out of the total of 8 gammas in this area, all but two fall between 1620 and 1680 kev.

2 The other two fall at 1887 and 1806 kev and have a combined yield of .00304. The combined yield of the

3 rest is .0524 with .0492 of this falling between 1620 and 1630 kev. This implies an energy of 1625 kev

4 should accommodate the majority of the interference in this region even though the biggest peaks fall

5 outside the actual ROI.

6

7 The coefficient k5 is the uranium interference on the thorium ROI. There are no gammas listed for this

8 energy region from uranium. This implies the interference (and thus k5) will be zero. Since it is no

9 harder to measure this factor from a point source, it will be measured and provide the factor is not

10 statistically different from zero, it will be ignored. Otherwise, the energy that would be used in a

11 calculation is simply 2614 kev, the centroid of the thorium region.

12

13 The coefficient k6 is the radium interference on the thorium ROI. The only isotope found in this vicinity

14 is 2448 kev. Therefore, that is the energy that will be used for this k-factor.

15

D.6 SOURCE DISTANCE

17 The distance between the source and the detector is an important perimeter that requires a little

18 clarification. When the calibration sources are counted, the distance is important only because of the need

19 to approximate a point detector. The N_o/ϕ term accounts for whatever distance is used in Equation 5.

20 Since the N_f/N_o term is a ratio, the distance is unimportant as long as all the measurements are made from

21 the same distance. It should be noted that the h in equation 10 should still be the detector height not the

22 source distance. This allows the appropriate importance to be put on the individual angles.

23

24 When the uranium, thorium and radium sources are counted for the k-factor determination, they should be

25 counted at a distance equal to the distance used for the Nf/No determination. This is necessary because

26 all of the theory discussed in this report applies to a point detector. Since the ratio for the k-factor will be

27 multiplied by Nf/No, the No should be determined for the same distance. The difference in air

28 attenuation between the normal detector height and the distance that the sources are counted must be

29 accounted for. This is true because the air attenuation will affect the lower energy peak more than the

30 higher energy peak. However, a distance of 150 cm in air will attenuate less than 1 percent of the

31 1001 kev peak and even less of the other peaks of interest. Therefore, while the attenuation should be

32 considered if a large distance is to be used, this affect can be ignored for a distance of 150 cm or less.

1 D.7 <u>SOURCES</u>

2 The efficiency calibration was performed with NIST traceable button sources. The source details are

3 included in the table below. These sources were counted at a distance of 150 cm from the center of the

4 bottom face of the detectors. The measurements included points throughout a forth of a sphere in

5 30-degree increments. The count time varied from 2 minutes to 5 minutes depending on the time between

6 the assay date and the date the counts were performed.

7

8 **POINT SOURCE DATA**

Isotope	Primary Energies (kev)	Activity (uCi)	Assay Date	Half Life
Cs-137	661.6	5.04 ± 0.17	2/23/2000	30.0 yrs
Sn-113	391.7	5.13 ± 0.17	2/23/2000	115.09 days
Y-88	898, 1836	10.43 ± 0.33	2/23/2000	106.63 days

9

10 The interference coefficients were determined using uranium-238, radium-226, and thorium-232 sources.

11 The sources were counted at a distance of 150 cm from the bottom face of the detector and at an angle

12 normal to the detector face. These sources were also used to determine the fraction of the peak of interest

13 that was actually accounted for by the ROI. Since the results of these determinations are ratios, the exact

14 quantity of each isotope is not important. It was only necessary to obtain separate sources of uranium,

15 radium and thorium. The actual sources used were the sources manufactured for the calibration pad. This

16 represents the only link between these two calibration methods but since the quantity is not important to

17 this calibration, it is an unimportant link. Details of these sources can be found in Appendix C.

18

19 D.8 <u>MEASURED VALUES</u>

20 As discussed earlier, the point source efficiency equation consists of three main parts. The N_f/N_o term,

21 the N_o/ϕ term and the ϕ/A term. Mathematically, this looks like:

22

23 $N_f/A = N_f/N_o * N_o/\phi * \phi/A$

24

25 The term N_f/A is the efficiency since N_f represents the net count rate and it is divided by a unit activity.

26 The last term is a purely mathematical term that determines the expected gamma flux at the detector from

27 an infinitely large homogeneous source of unit activity. The first two terms are measured as part of the

28 calibration. The next three plots show these factors as well as the efficiency (N_f/A) plotted against

29 gamma energy. The points include the measurements used to determine these factors as well as the

000083

1 interpolated values for the primary isotopes of concern. These values appear at 1001 kev, 1765 kev, and

2 2614 kev for uranium-238, radium-226, and thorium-232 respectively.

3

4 **Figure 1**

5
6
7
8 **Figure 2**

9
10
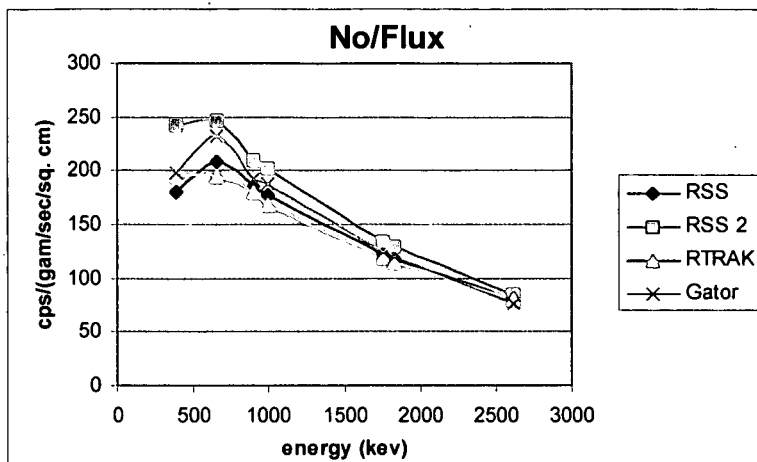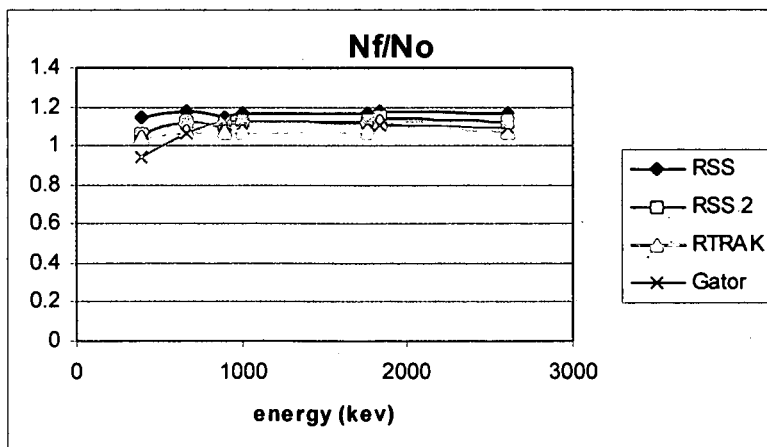
Figure 3
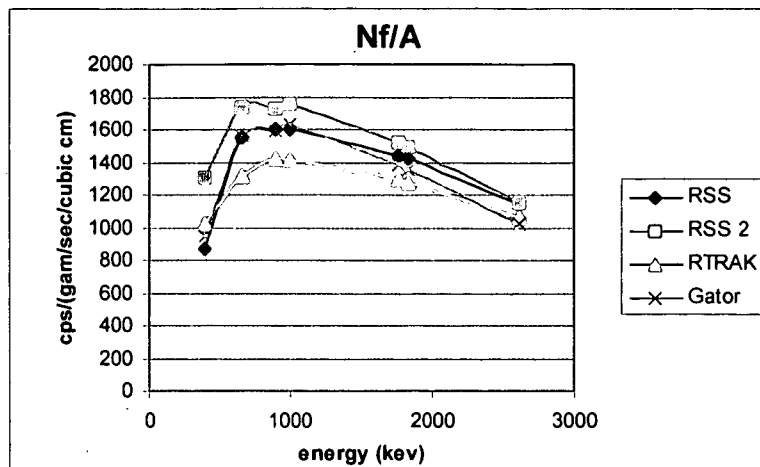
The full absorption peak factor discussed in section D.3 corrects the efficiency to what is actually measured with the ROI instead of the full absorption peak. The measured values of these factors are shown in the table below.

FRACTION OF FULL ABSORPTION PEAK ACCOUNTED FOR

Isotope	Energy (kev)	RSS1	RSS2	RTRAK	Gator
U-238	1001	0.484±.005	0.477±.009	0.561±.016	0.439±.012
Ra-226	1765	0.839±.020	0.934±.018	0.898±.020	0.910±.024
Th-232	2614	0.929±.019	0.925±.019	0.885±.018	0.930±.025

The radium-226 and thorium-232 values indicate that nearly 100 percent of the full absorption peak is accounted for in the ROI. This is true since the ROI can and is set very wide because there is little interference in that area to contend with. The uranium-238 peak accounts for less of the peak. This is necessary since interfering isotopes in or near this peak can have a large affect if more of the peak is included in the ROI.

The final resultant efficiency including the counting error is shown in the table below. These values include the correction for the full absorption peak.

EFFICIENCIES DETERMINED BY POINT SOURCE

Isotope	RSS1	RSS 2	RTRAK	Gator
U-238	0.242±.003	0.263±0.012	0.247±0.013	0.224±0.018
Ra-226	7.601±.187	8.933±0.542	7.343±0.463	7.908±0.851
Th-232	14.182±.319	14.223±1.136	12.494±1.019	12.681±1.806
K-40	5.212±.112	6.008±0.330	4.790±0.268	5.705±0.539

1 The next value determined was the interference coefficients. Section D-5 discusses these coefficients

2 breifly but a more detailed discussion can be found in Appendix A. In that appendix thirteen coefficients

3 are listed as F1 through F13. The purpose of these coefficients is to correct the net count rate of an ROI

4 to eliminate any counts from interference. The application of these coefficients is most easily understood

5 by showing the equations they are used in.

6

7 $U_{cnet} = U_{net} * F1 + Ra_{cnet} * F2 + Th_{cnet} * F3$

8 $Ra_{cnet} = U_{net} * F4 + Ra_{cnet} * F5 + Th_{cnet} * F6$

9 $Th_{cnet} = U_{net} * F7 + Ra_{cnet} * F8 + Th_{cnet} * F9$

10 $K_{cnet} = K_{net} * F10 + U_{net} * F11 + Ra_{cnet} * F12 + Th_{cnet} * F13$

11

12 The values measured for these coefficients are listed in the table below including the one sigma counting

13 error.

14

15 **INTERFERENCE COEFFICIENTS DETERMINED BY POINT SOURCE**

16

	RSS		RSS2		RTRAK		Gator	
F1	0.988	± 0.001	1.011	± 0.004	1.013	± 0.011	1.012	± 0.008
F2	0.129	± 0.009	-0.046	± 0.008	-0.032	± 0.012	0.004	± 0.010
F3	-0.104	± 0.019	-0.518	± 0.019	-0.587	± 0.030	-0.630	± 0.025
F4	-0.099	± 0.006	-0.100	± 0.015	-0.539	± 0.041	-0.140	± 0.026
F5	0.998	± 0.003	0.999	± 0.003	1.016	± 0.008	1.011	± 0.003
F6	0.505	± 0.025	0.507	± 0.024	0.795	± 0.045	0.437	± 0.032
F7	-0.007	± 0.003	-0.011	± 0.007	0.008	± 0.016	-0.025	± 0.013
F8	0.021	± 0.006	-0.012	± 0.005	-0.002	± 0.007	0.034	± 0.006
F9	1.011	± 0.003	1.000	± 0.004	0.995	± 0.010	1.027	± 0.009
F10	1.000	± 0.000	1.000	± 0.000	1.000	± 0.000	1.000	± 0.000
F11	-0.014	± 0.010	-0.003	± 0.018	0.146	± 0.039	-0.023	± 0.031
F12	-0.287	± 0.019	-0.230	± 0.016	-0.105	± 0.034	-0.165	± 0.019
F13	0.189	± 0.019	0.110	± 0.017	0.009	± 0.027	0.124	± 0.020

17

18

1 The calibration factors are then the interference coefficients above, divided by the efficiency. The results

2 are presented below.

3

4 **CALIBRATION COEFFICIENTS DETERMINED BY POINT SOURCE**

5

		RSS			RSS2			RTRAK			Gator		
U equation	U coefficient	4.088	±	0.050	3.849	±	0.179	4.093	±	0.216	4.508	±	0.371
	Ra coefficient	0.533	±	0.040	-0.174	±	0.031	-0.128	±	0.050	0.017	±	0.046
	Th coefficient	-0.431	±	0.079	-1.971	±	0.116	-2.371	±	0.171	-2.809	±	0.255
Ra equation	U coefficient	-0.013	±	0.001	-0.011	±	0.002	-0.073	±	0.007	-0.018	±	0.004
	Ra coefficient	0.131	±	0.003	0.112	±	0.007	0.138	±	0.009	0.128	±	0.014
	Th coefficient	0.066	±	0.004	0.057	±	0.004	0.108	±	0.009	0.055	±	0.007
Th equation	U coefficient	0.000	±	0.000	-0.001	±	0.001	0.001	±	0.001	-0.002	±	0.001
	Ra coefficient	0.001	±	0.000	-0.001	±	0.000	0.000	±	0.001	0.003	±	0.001
	Th coefficient	0.071	±	0.002	0.070	±	0.006	0.079	±	0.007	0.081	±	0.012
K equation	K coefficient	0.192	±	0.004	0.166	±	0.009	0.209	±	0.012	0.175	±	0.017
	U coefficient	-0.003	±	0.002	0.000	±	0.003	0.030	±	0.008	-0.004	±	0.005
	Ra coefficient	-0.055	±	0.004	-0.038	±	0.003	-0.022	±	0.007	-0.029	±	0.004
	Th coefficient	0.036	±	0.004	0.018	±	0.003	0.002	±	0.006	0.022	±	0.004

6

APPENDIX E

FIELD COMPARISON DATA

1
2
3

APPENDIX E
FIELD COMPARISON DATA

4 E.1 DATA ELIMINATED FROM FIELD COMPARISON

5 The two source calibrations in this document were compared to previously obtained field data. This data

6 consisted of a number of the original calibration points including some locations removed from that

7 calibration as outliers. It also included some additional points added since that time. This data set was

8 not intended to be all-inclusive; it is simply a representative sampling of the available data. As such,

9 some outliers continued to exist. These were evaluated and determined to exhibit a high degree of

10 heterogeneous contamination.

11

12 The degree of heterogeneity is important since the NaI instruments are calibrated to an infinitely large,

13 homogeneously contaminated geometry. When field counting with these instruments, the degree of

14 homogeneity is judged by mapping the indicated activity. In this manner, strongly heterogeneous areas

15 can be seen visually.

16

17 All data on all instruments associated with locations A3-6, A3-8, A3-13, and A13-3 were excluded from

18 the comparison of the calibrations with field data. All exhibited indications of a high degree of

19 heterogeneous contamination. At location A3-6, HPGe measurements were obtained at several detector

20 heights. The indicated activity from these measurements increased by factor of nearly three as detector

21 height raised from 15cm to 100cm. At locations A3-8, and A13-3 two RSS1 measurements were

22 obtained orientated 90 degrees apart. The net count rates from these two measurements varied by a factor

23 of approximately two for one or more isotopes. Location A3-13 had only one HPGe and one NaI

24 measurement at a time. However the activity calculated from the HPGe data using the various energy

25 gammas was examined. This examination indicates that the uranium activity at this location varies by

26 >60 percent between different energy gammas. If the area were homogeneous, the values would be

27 statistically the same. The thorium and radium values also indicated a lesser degree of heterogeneous

28 contamination

29

30 E.2 DATA USED IN FIELD COMPARISON

31 Below is the data used for the field comparison. This is the data that is plotted on the figures in section 4

32 of this document. All calculated values are in pCi/g.

RSS1 FIELD DATA RESULTS

Location	Uranium				Radium				Thorium			
	HPGe	Pad Cal	Point Cal	Current Cal	HPGe	Pad Cal	Point Cal	Current Cal	HPGe	Pad Cal	Point Cal	Current Cal
RSS-A9-1-2	3.6	15.0	11.9	6.4	0.7	0.7	0.6	0.7	0.8	0.8	0.8	0.8
RSS-A15-2-2	5.3	19.1	15.8	12.3	1.2	0.9	0.9	1.0	0.9	0.9	0.8	0.8
GATOR-18-1-2	8.8	2.1	-1.9	2.4	0.7	0.5	0.5	0.6	0.9	0.8	0.8	0.8
RSS-A11-4-3	14.0	23.0	19.7	11.6	0.8	0.7	0.7	0.8	1.0	1.0	0.9	0.9
VTST1-RSS1-0548	16.7	30.6	23.3	32.8	5.8	5.8	5.8	4.4	0.7	0.8	0.7	0.7
VTST1-RSS1-0550	16.7	42.9	35.6	32.3	5.8	6.4	6.4	4.4	0.7	0.9	0.8	0.7
RSS-A11-5-2	20.0	24.0	21.1	12.2	0.9	0.6	0.5	0.8	1.0	1.0	0.9	0.8
RSS-A11-3-2	23.0	28.9	26.1	15.0	0.9	0.5	0.5	0.9	1.1	1.0	1.0	0.9
Gator-A11-3-2	33.0	14.0	10.0	9.5	1.1	0.6	0.6	0.8	1.4	1.0	0.9	0.9
RSS-A3-7-4	250.0	229.9	209.1	113.6	18.0	20.7	20.8	12.8	3.3	4.0	3.5	2.2
RSS-A3-11-2	275.0	247.2	229.3	184.3	20.6	17.6	17.7	16.0	4.7	4.4	3.9	2.4
RSS-A3-14-2	286.0	269.4	251.9	163.5	20.3	18.8	18.8	13.9	4.5	4.4	4.0	2.5
RSS-A3-12-3	306.0	260.7	248.1	168.4	20.3	18.7	18.8	15.5	3.1	3.1	2.8	1.7
RSS-A3-9-4	320.0	300.3	275.7	176.2	20.0	20.9	20.9	16.2	5.2	6.1	5.5	3.4
RSS-A3-10-3	360.0	287.6	274.2	178.9	21.0	20.8	20.9	16.3	3.1	3.3	2.9	1.8
GATOR-A3-10-1	445.4	332.1	323.2	184.7	17.9	15.8	15.8	12.9	4.5	4.3	3.9	2.5

Below is the net count rate data for the RSS1 field spectra used in the comparison. The table includes net count rate data for each isotope of concern. The columns labeled "new U-238" and "new Ra-226" are the result of improved ROIs. The two source calibrations are using these new ROIs while the current calibration uses the current ROIs. No change was made to the thorium-232 ROI.

000090

RSS1 FIELD DATA NET COUNT RATES

Location	U-238	New U-238	Ra-226	New Ra-226	Th-232
RSS-A9-1-2	4.69	4.05	3.28	-0.13	10.65
RSS-A15-2-2	7.50	4.87	5.13	1.57	11.51
GATOR-18-1-2	2.48	0.90	2.44	-1.61	11.00
RSS-A11-4-3	9.15	6.25	3.40	-0.49	12.99
VTST1-RSS1-0548	-5.16	1.57	29.81	39.28	9.51
VTST1-RSS1-0550	-4.69	4.05	29.18	44.10	10.29
RSS-A11-5-2	9.80	6.75	3.31	-1.76	12.91
RSS-A11-3-2	11.33	8.15	4.04	-2.42	13.70
Gator-A11-3-2	7.45	4.07	3.43	-1.73	13.18
RSS-A3-7-4	2.92	38.03	83.44	138.37	46.70
RSS-A3-11-2	36.29	47.03	105.19	112.49	53.15
RSS-A3-14-2	37.51	51.41	89.76	121.48	53.36
RSS-A3-12-3	22.19	47.65	104.12	129.42	36.45
RSS-A3-9-4	35.49	58.80	102.78	126.95	75.07
RSS-A3-10-3	25.07	52.22	109.23	144.86	38.28
GATOR-A3-10-1	63.31	71.54	82.75	100.70	53.34

The data used in producing the plots for the RTRAK and the Gator are included below.

RTRAK FIELD DATA RESULTS

Location	Uranium				Radium				Thorium			
	HPGe	Pad Cal	Point Cal	Current Cal	HPGe	Pad Cal	Point Cal	Current Cal	HPGe	Pad Cal	Point Cal	Current Cal
RSS A9-1	3.2	-16.0	-19.5	7.6	0.7	0.7	1.1	0.9	0.9	0.9	0.9	0.8
RSS A11-3	23.0	8.9	-1.9	17.3	0.9	0.5	0.6	1.0	1.1	1.1	1.1	0.9
RSS A3-11	275.0	196.9	110.4	275.5	20.6	23.3	24.5	21.5	4.7	5.4	5.3	3.0
RSS A11-5	20.8	-0.6	-8.6	12.6	0.9	0.6	0.9	0.9	1.1	1.1	1.0	0.8
RSS A11-4	14.3	-6.6	-13.7	11.7	0.8	0.5	0.8	0.9	1.0	1.1	1.1	0.9
RSS A11-4	14.3	-12.4	-18.0	12.4	0.8	0.5	0.9	1.0	1.0	1.1	1.0	0.9
RSS A11-5	20.8	-10.9	-17.3	12.1	0.9	0.7	1.2	0.9	1.1	1.2	1.1	0.9
RSS A3-10	361.5	476.0	342.8	310.6	21.2	22.3	19.6	19.6	3.2	3.2	3.2	1.8
RSS A3-7	243.0	146.2	87.5	175.0	18.2	18.6	19.4	14.4	3.3	3.3	3.2	1.9
RSS A3-9	313.0	197.4	106.0	231.8	19.9	23.9	25.2	17.5	5.2	6.0	5.9	3.3
RSS A3-12	306.0	96.8	53.1	115.1	20.3	24.8	26.8	10.6	3.1	2.9	2.8	1.7
RSS A3-14	286.0	82.7	37.8	5.3	20.3	23.2	25.3	2.0	4.5	3.5	3.4	2.1
RSS A15-2	5.2	-21.9	-25.3	11.5	1.2	0.7	1.3	1.1	0.9	1.1	1.0	0.9
PBC-8	0.9	-8.4	-12.5	5.6	0.6	0.7	1.0	0.7	0.6	0.8	0.7	0.7
PBC-9	2.3	-14.6	-17.7	5.3	0.7	0.6	1.0	0.7	0.7	0.8	0.8	0.7
PBC-1	0.0	-16.4	-18.2	4.0	0.6	0.5	0.9	0.6	0.6	0.7	0.7	0.7
PBC-6	24.8	16.0	4.8	17.0	0.8	0.6	0.7	0.9	0.9	1.0	0.9	0.8
PBC-4	17.8	-4.4	-11.2	12.2	0.7	0.8	1.1	0.9	0.9	1.0	1.0	0.8
PBC-5	14.4	-6.2	-12.5	8.4	0.7	0.5	0.8	0.8	0.9	1.0	1.0	0.8
PBC-10	22.6	-147.4	-174.7	44.6	1.9	1.3	4.7	3.0	7.3	7.9	7.5	4.3
PBC-7	47.7	37.8	19.6	25.4	0.7	0.7	0.6	1.1	1.1	1.2	1.2	0.9
PBC-2	9.4	-25.5	-29.5	3.7	0.7	0.4	1.0	0.8	1.1	1.3	1.2	0.9

RTRAK FIELD DATA NET COUNT RATES

Location	U-238	New U-238	Ra-226	New Ra-226	Th-232
RSS A9-1	4.05	1.73	4.74	0.09	11.20
RSS A11-3	12.56	7.39	4.58	-2.14	13.68
RSS A3-11	69.43	70.40	142.19	162.48	66.24
RSS A11-5	9.19	5.20	4.07	-0.99	12.65
RSS A11-4	8.53	4.37	4.04	-2.17	13.46
RSS A11-4	8.00	3.14	4.94	-1.81	13.11
RSS A11-5	8.60	3.78	4.30	-0.42	13.83
RSS A3-10	106.02	111.86	132.66	170.40	39.36
RSS A3-7	37.84	49.09	95.99	134.50	40.59
RSS A3-9	69.86	73.62	112.33	163.44	73.58
RSS A3-12	19.22	39.39	69.51	186.66	35.56
RSS A3-14	3.49	39.02	7.16	170.22	42.25
RSS A15-2	6.64	1.41	5.45	-0.19	13.09
PBC-8	3.51	2.37	3.55	1.06	9.29
PBC-9	3.66	1.49	3.35	-0.07	10.02
PBC-1	2.82	0.61	2.97	-0.11	8.75
PBC-6	12.32	7.96	4.36	-0.25	11.72
PBC-4	8.82	4.37	4.06	0.80	12.23
PBC-5	6.14	3.88	3.60	-1.51	12.06
PBC-10	44.47	11.06	5.95	-33.94	94.58
PBC-7	18.61	13.37	5.23	-0.19	14.84
PBC-2	3.52	1.51	2.95	-3.88	15.25

GATOR FIELD DATA RESULTS

Location	Uranium				Radium				Thorium			
	HPGe	Pad Cal	Point Cal	Current Cal	HPGe	Pad Cal	Point Cal	Current Cal	HPGe	Pad Cal	Point Cal	Current Cal
VTST1-Gator-0067	16.7	16.5	-6.3	54.2	5.8	5.6	4.8	4.6	0.7	0.9	0.7	0.8
Gator -A9-1-3	3.0	19.1	-9.6	30.1	0.8	0.7	0.6	1.7	0.8	0.8	0.7	0.9
Gator -A9-1-4	3.0	-3.3	-21.1	28.4	0.8	0.7	0.6	1.9	0.8	0.8	0.7	0.9
Gator -A11-3-4	23.9	28.0	-13.8	38.1	0.8	0.7	0.6	2.0	1.0	1.1	1.0	1.3
Gator -A3-11-1	175.0	149.9	-7.5	154.2	12.1	12.0	10.3	10.6	3.9	3.9	3.3	4.0
Gator -A3-10-3	445.4	380.3	114.5	184.4	17.9	21.6	18.5	12.5	4.5	4.1	3.4	3.9
Gator -A3-7-2	249.1	172.9	26.2	90.8	13.0	13.1	11.2	7.1	4.0	3.1	2.6	3.1
Gator -A3-9-2	337.8	286.4	54.5	130.8	17.2	19.8	16.9	9.9	5.2	4.6	3.8	4.5
Gator -A3-9-3D	337.8	299.4	67.3	119.3	17.2	20.0	17.1	9.0	5.2	4.3	3.6	4.2
Gator-15-1-1	29.1	49.8	-1.3	38.3	0.9	0.6	0.5	1.6	1.0	1.0	0.9	1.2
Gator-18-1-1	8.8	11.0	-17.5	31.6	0.7	0.6	0.5	1.8	0.9	0.9	0.8	1.1

GATOR FIELD DATA NET COUNT RATES

Location	U-238	New U-238	Ra-226	New Ra-226	Th-232
VTST1- Gator-0067	-4.81	3.47	14.23	34.17	8.03
Gator -A9-1-3	3.74	3.20	1.68	1.07	8.55
Gator -A9-1-4	0.69	0.79	2.70	1.03	8.78
Gator -A11-3-4	7.63	4.64	2.61	0.11	12.36
Gator -A3-11-1	17.54	22.64	38.45	66.29	39.41
Gator -A3-10-3	20.90	48.91	46.92	134.92	38.57
Gator -A3-7-2	3.38	24.13	23.71	77.73	29.89
Gator -A3-9-2	9.04	39.09	35.20	118.81	44.07
Gator -A3-9-3D	8.37	40.19	31.45	121.15	41.27
Gator-15-1-1	10.48	6.92	1.17	0.18	11.57
Gator-18-1-1	4.02	2.51	2.15	-0.41	10.24